5-2002

The design and analysis of circular rings for splicing sign columns

Derrick L. Baird
University of Tennessee

To the Graduate Council:

I am submitting herewith a thesis written by Derrick L. Baird entitled "The design and analysis of circular rings for splicing sign columns." I have examined the final electronic copy of this thesis for form and content and recommend that it be accepted in partial fulfillment of the requirements for the degree of Master of Science, with a major in Mechanical Engineering.

John Landes, Major Professor

We have read this thesis and recommend its acceptance:

Accepted for the Council:
Carolyn R. Hodges

Vice Provost and Dean of the Graduate School

(Original signatures are on file with official student records.)

To the Graduate Council:

I am submitting herewith a thesis written by Derrick Baird entitled "The Design and Analysis of Circular Rings for Splicing Sign Columns." I have examined the final paper copy of this thesis for form and content and recommend that it be accepted in partial fulfillment of the requirements for the degree of Master of Science, with a major in Mechanical Engineering.

John D. Landes

John Landes, Major Professor

We have read this thesis and recommend its acceptance:

Accepted for the Council:

Vice Provost and Dean of Graduate Studies

The Design and Analysis of Circular Rings for Splicing Sign Columns

A Thesis Presented for the Master of Science Degree
The University of Tennessee, Knoxville

Derrick L. Baird

May 2002

Dedication

This thesis is dedicated to my wife and daughter, Leigh Ann and Elizabeth Baird, whose time I borrowed and can never repay, my father, Archie Baird, a great role model for work ethic, my stepmother, Alma Baird, always supportive, to my mother, Vonna Gail Baird, I hope she would be proud, and to the rest of my family for their support.

Acknowledgements

I would like to thank my wife Leigh Ann for giving me the time to complete my degree especially here at the end. I thank Dr. Landes for his guidance in preparing this document and the interesting post gradate classes of his I have taken. I thank Dr. Iannelli for the being a teacher and Dr. Boulet for three dimensional dynamics and serving on my committee on such short notice.

Abstract

Circular rings are used extensively in the sign industry to splice columns of different sizes together. Typically two or three rings are used to splice the columns. Due to the complex geometry no straightforward design approach is applicable. The scope of this thesis limits the applied load to that from lateral wind pressure only.

To analyze the rings an indeterminate static model is applied in spreadsheet form. The analysis is greatly simplified by only using four effective sections of the ring. The virtual sections are rectangular shaped and defined by a variable angle. The top column is treated as a rigid beam and the effective sections as springs. Finite element models are created to determine the actual stress in the rings. The stresses found in the finite element models are made to equal the stresses for the spreadsheet model by adjusting the angle defining the effective section. The angle and variables used in the model are entered into a statistical analysis platform to determine an approximation for the effective section angle. The approximation of the angle is entered in the spreadsheet model and the approximate stress is compared to the stress found from finite element analysis.

The effective section method is applicable to designing circular rings if used with the approximation of effective section angle. Many configurations can be analyzed quickly with the approximation in spreadsheet form. The rigidity of the top column has more affect on the ring stress when the inertia of the top column is low. This result requires that larger factor of safety be used when the top column is small. The highest stress areas of the rings are the sections in tension and compression which lie in the same plane as the direction of applied lateral load. The percent difference between the actual and approximate stress averaged 9.2 percent for the top and bottom rings and 12.7 percent for the middle ring when used. The section angle required ranged between 2.8 and 21.5 degrees for the configurations tested here.

Table of Contents

List of Tables

List of Figures

Chapter One

Introduction

Background

In the sign industry it is common to splice two different sized columns using two or three plates spaced some distance apart (see figure 1). Pipes are the common choice for these columns, but square and rectangular tubes are also used. Plates are placed at the bottom of the smaller top column perpendicular to the length and attached inside the top of the bottom column. All the plates are attached to the top column by continuous fillet welds on the top side of the plates. The cap plate is connected to the top of the bottom column by a continuous fillet weld. The cap plate is larger in diameter than the bottom column and overhangs by at least three-sixteenths of an inch to allow for the fillet weld. The lower plates are made one-eighth inch smaller in diameter than the inside diameter of the bottom column. The lower plates are connected around the plate perimeter using no less than four plug welds through slots in the bottom column.

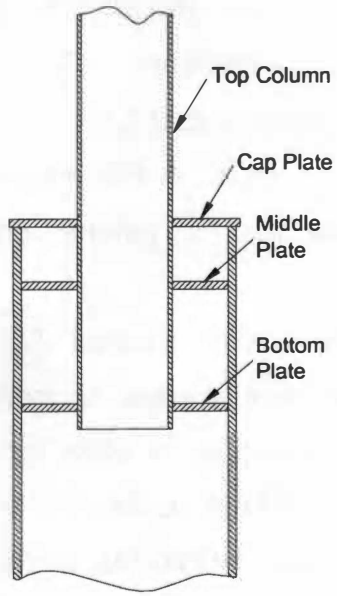

Figure 1 – Section Splice

There are two types of loads transferred through the plates, axial and lateral force (see figure 2). Axial force, W, develops from the weight of everything connected to the plates above the bottom column. This weight is typically from sign cabinets and the top column self weight. Additional weight can be introduced from snow loading if the axially projected area of everything above the plates presents a large enough surface area. Reaction to the axial load is only transferred through the cap plate. This is due to the assembly

procedure used. The upper column and attached plates are lowered down on top of the bottom column resting all the weight on the cap plate. The cap plate is then welded completely. The lower plates are then plug welded to the bottom column.

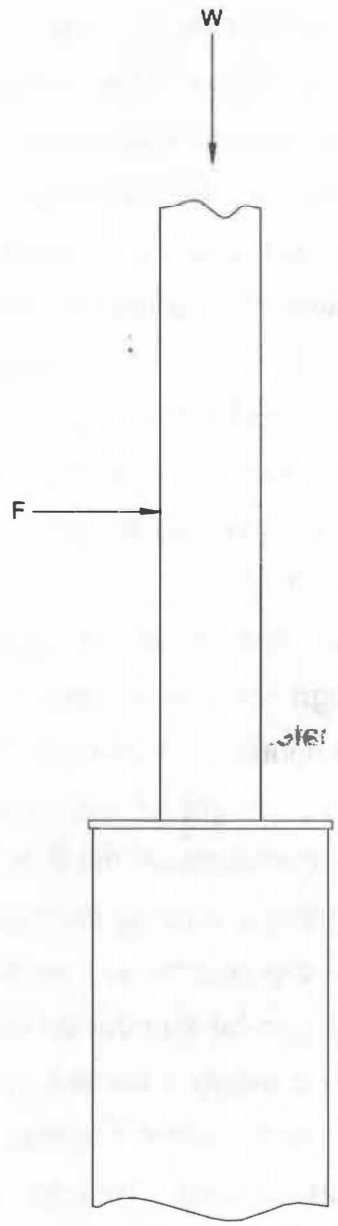

Figure 2 – Column Loading

Lateral force, F, is developed by pressure from the wind on the projected area of the column and appendages above the plates and acts perpendicular to the column axis. Lateral load is transferred through all the plates since the plates are under little to no pressure from the wind when attached to the bottom column. The loading developed from lateral force is transferred to the plates by a moment and transverse shear. These loads are much greater in magnitude relative to that of the axial loads.

In text written specifically for the sign industry [1] these plates are addressed from a welding standpoint only and the spacing has been determined by past experience. The author's model utilizes two rings spaced 1.5 to 2 times the top column diameter apart. A thin middle ring is used only to guide the top column on during assembly.

The current design method [2] utilizes three plates. The middle plate is located low enough below the cap plate to allow for welding access. The lower plate is located 1.5 times the upper column diameter below the middle plate. The thicknesses of the two lower plates are

determined by using the reactions (R1 and R2) of a simply supported beam with a force applied to one end (see figure 3) and determining the stress in two small sections of the plate through which the reactions pass (see figure 4) and analyzing them as axially loaded members.

The effective ring section is rectangular in shape and the width is taken so that it subtends an angle of thirty degrees at the center of the column. The length of the section is the distance between the inside and outside radius of the ring (see figure 5). The thickness of the plates is then determined based on the allowable stress in the axially loaded members. A factor of safety of 2 is then applied.

The thickness of the cap plate is determined by treating the effective section (see figure 4) as a cantilever beam and calculating the flexural stress from only the axial load. A factor of safety of 2 is applied to the allowable stress and compared to the flexural stress to determine adequacy. This method has been used effectively for a number of years, but a more in-depth study has been needed to perhaps reveal a more efficient use of plate and column material and bring some validity to the previous approach.

The use of an effective section is good in that it allows the rings to be analyzed with simpler equations from mechanics of materials. Finite element analysis is used routinely in mechanics problems such as this where the geometry is complex and the analysis is too cumbersome to be routinely repeated.

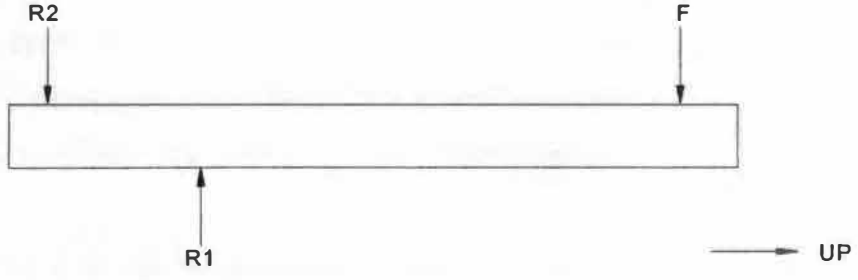

Figure 3 – Simple Supported Beam

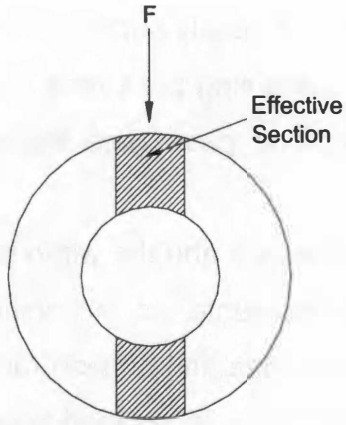

Figure 4 – Two Ring Sections

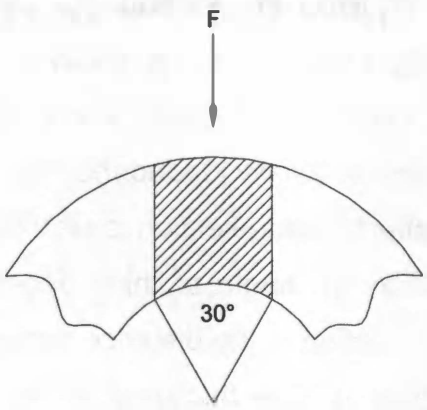

Figure 5 – Single Ring Section

By combining these two approaches an accurate model can be determined. The angle defining section width used in an indeterminate static model can be adjusted to equal the stress found in the finite element approximation. With the model in spreadsheet form, independent variables affecting stress can be easily changed and many different configurations can be evaluated.

Problem Statement

It is the goal of this thesis to develop a spreadsheet model to accurately determine the stress in ring plates that resist lateral wind loading on spliced cylindrical columns and thereby make the design of these rings quicker with more efficient use of material. The scope of this thesis is limited to steel columns of circular cross section since pipes are used in the majority of sign constructions.

In a typical design the stress created in the rings cannot exceed the allowable stress to be deemed acceptable. Spacing of the rings cannot be excessive in an effort to minimize the ring thickness and vice versa. The model will be implemented in spreadsheet form to allow for easily changing the variables.

By using the effective section a simpler rectangular element is created and analyzed. The ring itself is a plate which requires the use of the more

complicated theory of elasticity to be analyzed. Simpler elements such as the virtual rectangular elements created by the effective section can be analyzed with the mechanics of materials method. The angle used to define section width will be left variable to allow matching of the stress in the spreadsheet to that of the finite element approximation.

Procedure of Study

A spreadsheet model will be developed using the idea of effective ring section defined by a new arbitrary angle theta. The rings will be divided into four effective sections virtually rectangular in shape (see figure 6). The top column will be treated as a rigid beam and the effective sections of the rings will be analyzed as axial and flexural components.

Stiffness of the effective sections will be used to determine the reactions in an indeterminate static model. Stress in each section will be calculated based on the section stiffness and the force acting on the section. A finite element model will be created to determine the stresses in the rings. In an effort to cover the variety of columns, ring spacing, and thicknesses that can occur, twenty-seven individual cases will be created. Differences between the cases will be made by varying the top column wall thickness and diameter, bottom column wall thickness and diameter, number of rings, ring thickness, distance between rings, and the moment and force applied.

The angle that determines the section width will be left variable to allow matching of the maximum stress determined in the spreadsheet model to that found in the finite element model. Statistical analysis will be used to find variable effects unaccounted for in the model. Parameter estimates from the statistical model will be used to approximate the effective section angle. Finally, results of the cases will be examined along with comparisons of the actual to approximate stress.

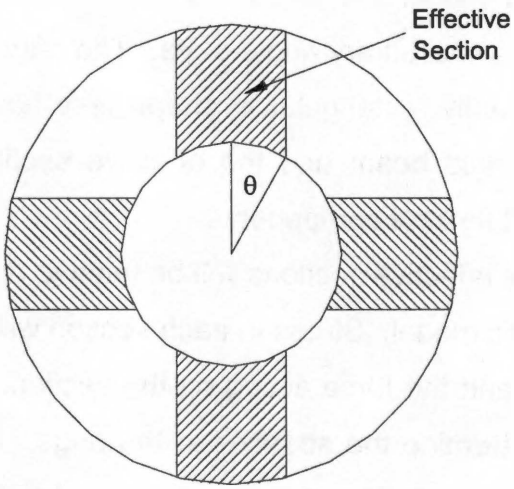

Figure 6 – Effective Ring Section

Chapter Two

Spreadsheet Model

Static Model

The statically determinate model used for the top column and rings consists of a rigid beam with two reactions to the applied lateral force (see figure 7). These reactions are a result of the rings attachment to the top column. The lateral force is derived from the wind loading.

Wind loading is a distributed pressure on the projected area of the sign and column. The pressure is determined by the building code used in the jurisdiction of the locality where the sign is placed. The most commonly agreed upon code is ASCE 7-98 [4]. It presents the calculations for wind pressure based on maximum velocity of a 3 second gust occurring within a 50 year period. The velocity data is collected by weather stations throughout the United States. Structure type, terrain, and height above grade are some of the variables also used in determining pressure. Typically the pressure will be around 30 psf, but can be more than double that in a hurricane prone region.

Wind pressure is multiplied by the sign and column width to generate a linearly distributed load. The moment from that load is determined at the cap

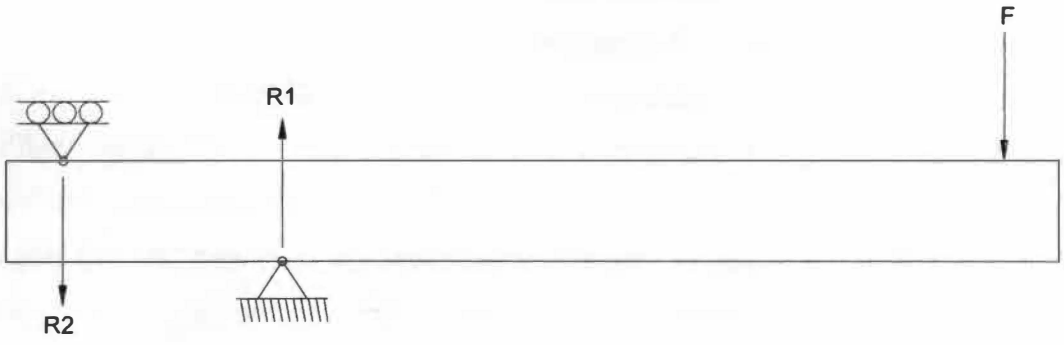

Figure 7 – Top Column Static Model and Reactions

plate by treating the column as a cantilevered beam with distributed loading (see Figure 8).

To derive the location of a single force at some distance up the column, the moment at the cap plate is divided by the shear at the cap plate. The magnitude of the single lateral force is equal to the magnitude of the shear at the cap plate. Reactions at the rings are determined by summing the moments and forces and are found to be,

$$R_1 = F + R_2 \qquad \text{(Equation 1)}$$

$$R_2 = F \cdot d/l \qquad \text{(Equation 2)}$$

where d is the distance between the rings and l is the distance between F and R_2.

Indeterminate Model

A more accurate description of the ring reactions can be found through the use of indeterminate statics [5]. The ring sections are treated as springs fixed to ground and the column is assumed rigid and rotating about the center of rigidity of the rings (see figure 9). The lateral loading on the column is found in the same manner as the determinate static model. To find the center of rotation, the stiffness of each effective ring section must be determined.

Sections of the rings are assumed to be virtually rectangular bars and designated top, bottom, front, and back (see figure 10). The section width is determined by the independent variable theta. The section thickness is the same as the ring thickness. Section length is the distance between the top column outer radius and bottom column inner radius parallel with the section axis at the intersection of the angle theta (see Figure 11). See Appendix A for geometric developments for section length.

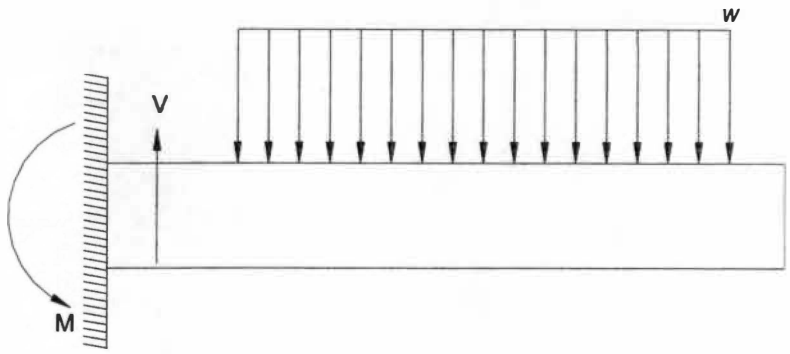

Figure 8 – Top Column Cantilever Model

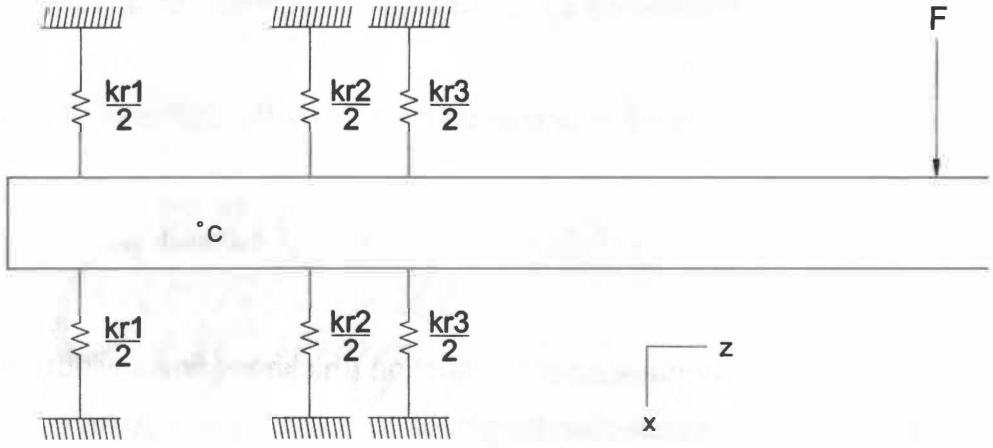

Figure 9 – Indeterminate Static Model

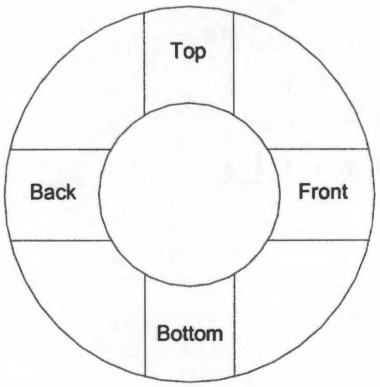

Figure 10 – Section Nomenclature

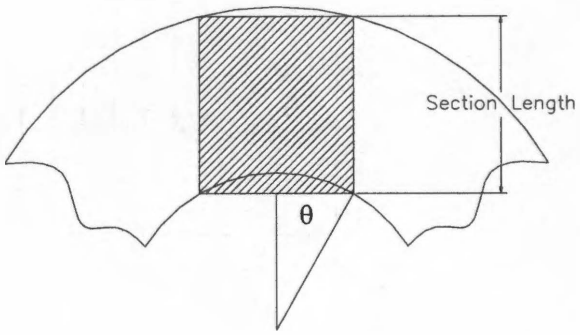

Figure 11 – Effective Section

The top and bottom sections are the axial components of the ring. Front and back sections are considered flexural components of the ring. The effective stiffness of the ring is determined by combining the stiffness of all four sections and is developed as follows.

For the stiffness of the top and bottom sections the stiffness of an axially loaded column is used,

$$k_a = A \cdot E / L \qquad \text{(Equation 3)}$$

where A is the cross-sectional area of the section (thickness times width), E is the elastic modulus, and L is the section length.

For the stiffness of the right and left sections the stiffness of a cantilever beam in flexure is used,

$$k_b = 3 \cdot E \cdot I / L^3 \qquad \text{(Equation 4)}$$

where I is the area moment of inertia of the cross-section about the strong axis.

Since the deflections of the four effective sections are equal the total stiffness of all four sections is (see Figure 12),

$$k_r = 2 \cdot \left(3 \cdot E \cdot I / L^3 + A \cdot E / L \right) \qquad \text{(Equation 5)}$$

With the total ring stiffness known the center of rigidity [6] is found by summing the ring to rotation center distance times the stiffness and dividing by the sum of the stiffness,

$$\overline{z_k} = \frac{\sum_{n=1}^{3} k_{rn} \cdot d_n}{\sum_{n=1}^{3} k_{rn}} \qquad \text{(Equation 6)}$$

With the assumption that the column is a rigid beam and rotates about the center of rigidity the deflections of the ring sections can be related to one another by similar triangles,

$$\frac{\delta_1}{d_{c1}} = \frac{\delta_2}{d_{c2}} = \frac{\delta_3}{d_{c3}} \qquad \text{(Equation 7)}$$

where δ and d_c are the deflection and distance defined in figure 13.

The deflection and stiffness are used to find the force transferred to each ring,

$$F_n = \delta_n \cdot k_n \qquad \text{(Equation 8)}$$

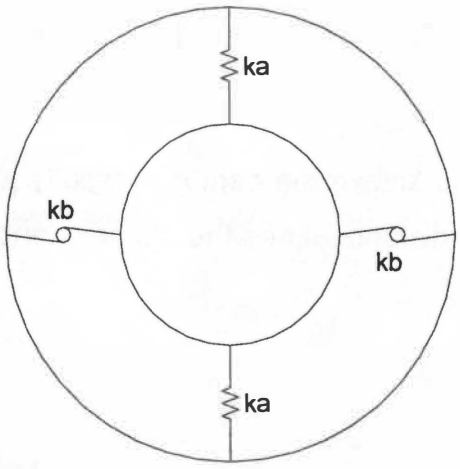

Figure 12 – Section Stiffness

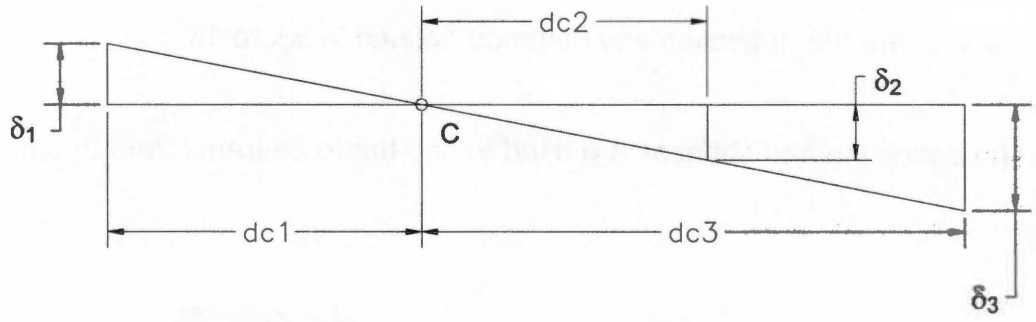

Figure 13 – Similar Triangles Diagram

The final equations needed to solve for the ring section reactions are the sum of forces and moments acting on the column (see figure 14).

$$\sum F_X = F + F_1 - F_2 - F_3 \qquad \text{(Equation 9)}$$

$$\sum M_c = F \cdot d_{cf} + F_1 \cdot d_{c1} - F_2 \cdot d_{c2} - F_3 \cdot d_{c3} = 0 \qquad \text{(Equation 10)}$$

By solving these equations simultaneously the ring reactions are found to be,

$$F_2 = k_2 \cdot \left(\frac{F \cdot (d_{c1} + d_{cf}) \cdot d_{c2}}{d_{c1} \cdot (d_{c2} \cdot k_2 + d_{c3} \cdot k_3) + {d_{c2}}^2 \cdot k_2 + {d_{c3}}^2 \cdot k_3} \right) \qquad \text{(Equation 11)}$$

$$F_3 = \frac{F \cdot (d_{c1} + d_{cf}) - (d_{c1} + d_{c2}) \cdot F_2}{d_{c1} + d_{c3}} \qquad \text{(Equation 12)}$$

$$F_1 = F_2 + F_3 - F \qquad \text{(Equation 13)}$$

Ring Section Stress

Each section of the ring has its own independent stress. The stresses in the top and bottom sections are equal and are determined by,

$$\sigma_b = M_s \cdot y_s / I_s \qquad \text{(Equation 14)}$$

where M_s is the moment at the base, y_s is the distance to the outer fiber of the section, and I_s is defined in below equation 4. Stresses in the front and back sections are also equal and determined by,

$$\sigma_a = F_s / A_s \qquad \text{(Equation 15)}$$

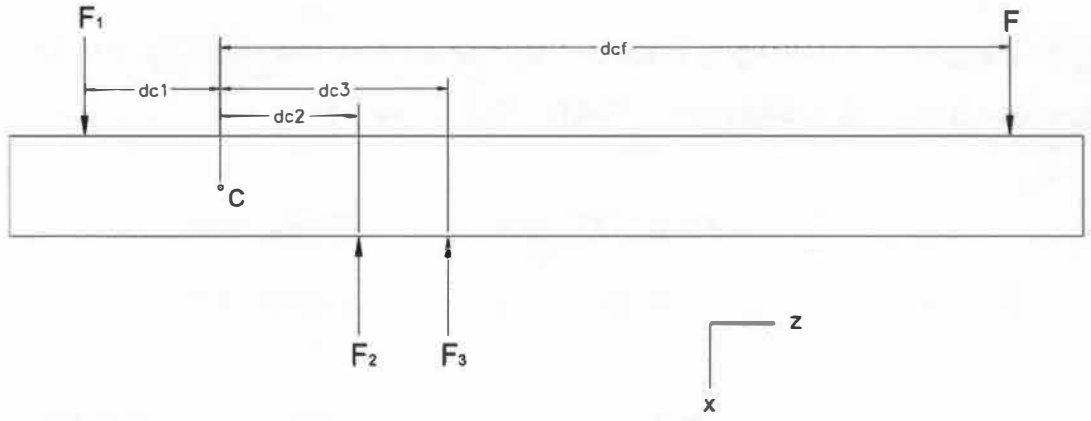

Figure 14 – Indeterminate Model Reactions

The force and moment in equations 14 and 15 are found by taking the ratio of the stiffness of the section compared to total stiffness of all four effective sections and multiplying by the total reaction force at the location.

Since the column is assumed to act as a rigid beam rotating about the center of rigidity, a small deflection in the z-direction also occurs in the top and bottom sections (figure 15). The stress created from this deflection is flexural. The top and bottom sections are treated as cantilever beams and the resultant stress is combined with the axial stress. Developments for this addition are located in the appendix. A small deflection also occurs in the z-direction of the side sections and is ignored.

Spreadsheet Assembly

Now that all the equations have been developed the spreadsheet model is ready to be assembled. All of the variables and equations are entered in individual columns moving from left to right. All variables are entered first with section angle being the last. The lateral force location and moment at the cap plate are also entered.

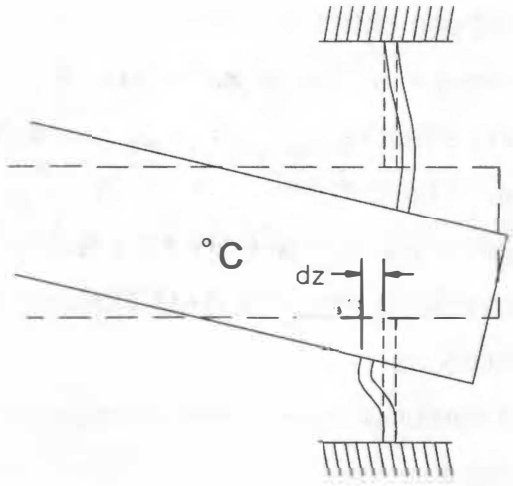

Figure 15 – Deflection in z-direction of Axial Section

Position of the lateral force is located 96 inches above the cap plate for all models. Pipes are constructed typically in 20 foot, 30 foot, and 40 foot lengths. Assuming that the column is 20 foot long with a uniformly distributed load the lateral force location would be located at 120 inches from the cap plate. The load is brought down another 24 inches to typify a worst case lateral load location. Since, the moment will be the same for any lateral load location moving it down will increase the shear.

The magnitude of lateral force is determined by taking 90 percent of the moment needed to bring the stress in the column to the allowable stress defined by the ASD Manual. Allowable stress is found by taking the yield of the column and multiplying by .66 then increasing that number by 4/3 since the force is due to wind loading. The yield of the pipe is typically 35 ksi resulting in a 30.8 ksi allowable stress. The lateral force is determined by the equation,

$$F = \frac{.9 \cdot 30.8ksi \cdot S}{96in.} \qquad \text{(Equation 16)}$$

where S is the section modulus of the pipe.

After the variables have been entered, the next section of the spreadsheet is used to calculate the geometry of the sections and the resultant section properties. The stiffness of the effective sections, total ring stiffness and center of rigidity are calculated next. The deflections at all the rings are determined using similar triangles. The forces and stresses are calculated in the final section of the spreadsheet. See Appendix B for a complete layout of the spreadsheet and the formulas used in calculations.

Twenty-seven different combinations of eleven independent variables will be evaluated. Besides increasing the sample population used for statistical analysis, this many samples allows trends to be evaluated among groups of three cases where only one or two independent variable are changed.

Chapter Three

Finite Element Model

Model Configuration

Each of the twenty-seven cases has a corresponding finite element model. Each finite element model consists of the upper column and the rings (see figure 16). The column again is 96 inches long above the cap plate and divided into 12 elements in the z direction and 40 elements around the circumference. Each element is a plate with a node at each of the four corners. Each column plate element has the same thickness as the pipe wall. Where the nodes on the rings are to be located the nodes on the column elements must also be located. To obtain model continuity at the ring's inner radius the column and ring nodes must collocate. Below the cap plate the column is divided into equal length elements corresponding to the ring locations. The column is made to extend past the bottom ring some arbitrary distance, usually one or two plate element lengths (see figure 17).

The rings are divided into 40 elements around the circumference so that the nodes correlate to those on the column. In an effort to make the plate elements more square the ring is divided into four elements between the inner and outer radii. Ring plate element thickness corresponds to the actual ring thickness.

Boundary Conditions and Loading

Boundary conditions are applied to the model in an effort to emulate actual boundary conditions in the worst case. The cap plate is welded all around its circumference and all other plates are attached with a minimum of four plug welds equally spaced around the column perimeter. Four plug welds represent

the worst boundary condition that can be applied. This is because more of the

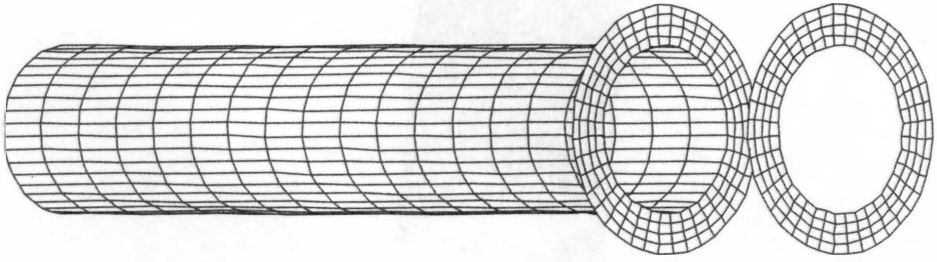

Figure 16 – Column and Rings Configuration

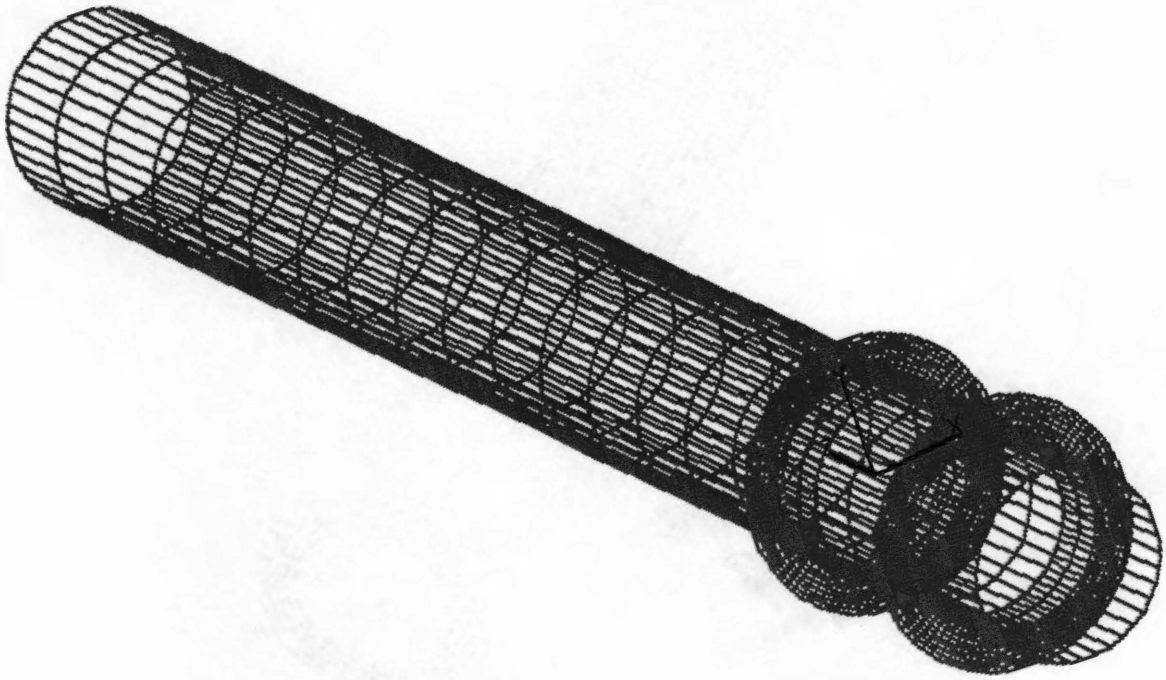

ring is left free at the ring outer radius allowing the majority of the load to pass through a smaller section of the ring. The four plug welds are centered on the x and y axis in both the positive and negative direction. Nodes around half the perimeter centered on the negative x axis are acted on by springs in the positive x direction. This approach is used to model bearing of the bottom ring on the inside of the bottom column. To emulate the perimeter plug weld five nodes are fixed at the outermost x direction (see figure 18). All rings attached by plug welds have this configuration. It is evident that the lower plates have the weakest type of attachment to the bottom column. This configuration is also applied to the cap plate only rotated one hundred eighty degrees to the bottom ring orientation (see figure 19).

Loading on the column is the same point load used in the spreadsheet model. Again in an effort to use the harshest case the total load is applied in the positive x direction to a single node at the extreme negative x location 96" above the cap plate (see figure 20).

Model Refinement

To obtain more accurate results ring stress is tested for convergence by refining the mesh. Case one is refined by dividing the ring elements into smaller pieces until further refinement does not yield significantly different results. It is seen that refinement of the top column in the area of the ring is also effective. The use of eighty elements around the perimeter of the ring and eight elements in the radial direction is found to be sufficient.

All ring models originate as forty elements in the theta direction and four elements in the radial direction. Each element is then divided in half in both directions. This type of refinement leaves the original nodes connected between the column and ring with a free node in-between the connected nodes. A more true to life configuration would have each node connected since the inside radius of the ring is welded all around to the column. By leaving half the interior radial

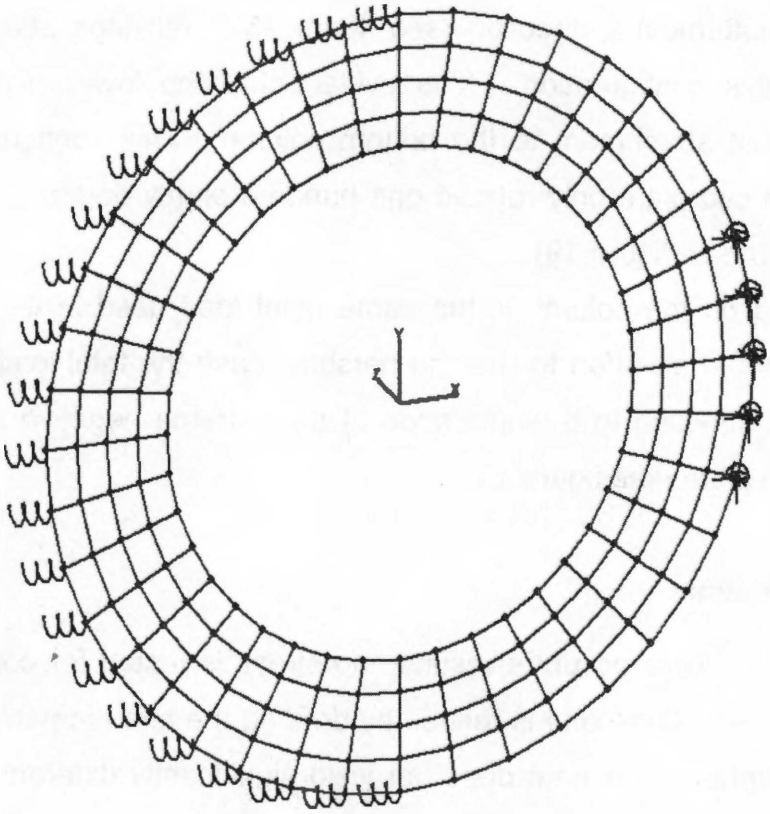

Figure 18 – Nodal Conditions of the Bottom Plate

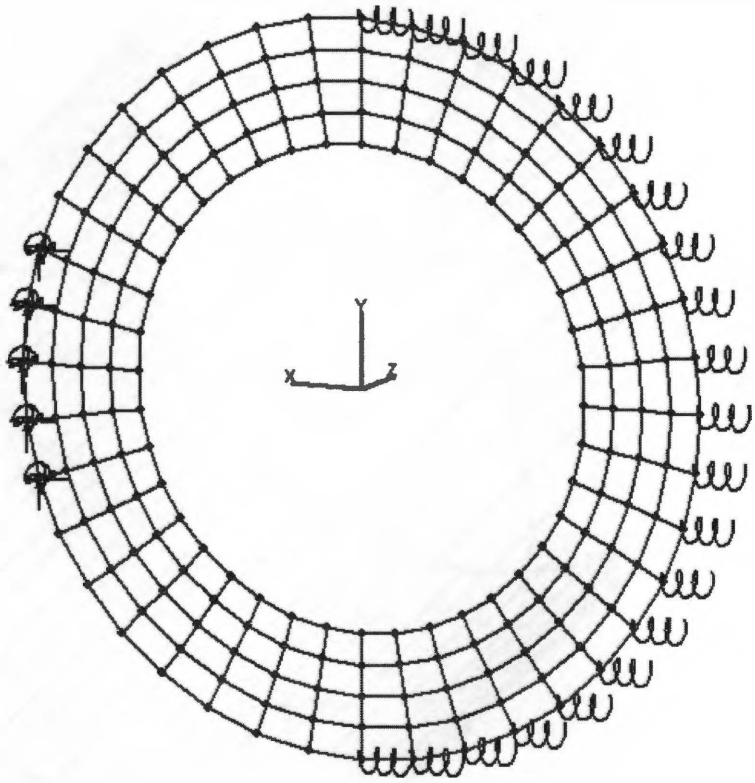

Figure 19 – Nodal Conditions of Top Plate

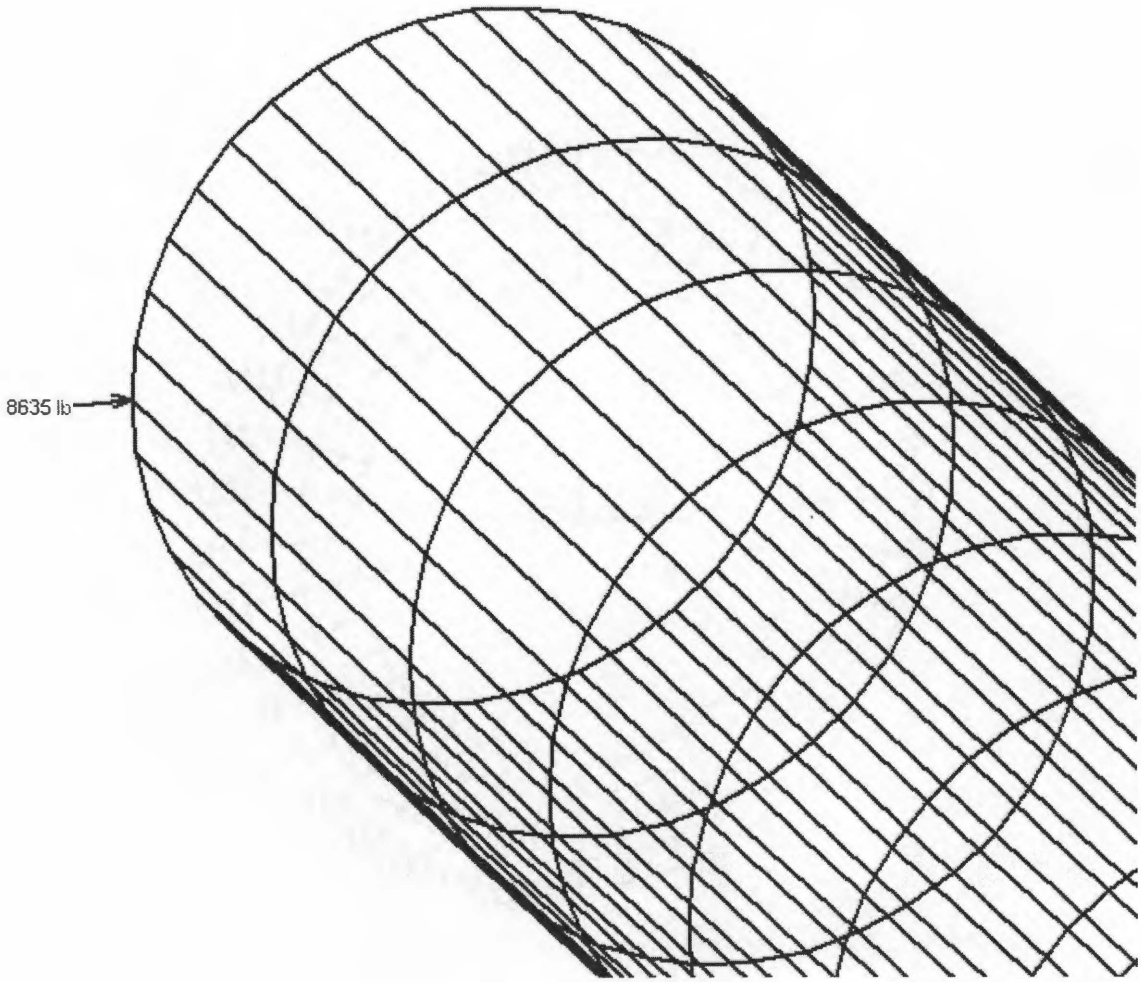

Figure 20 – Location of Applied Nodal Force

nodes disconnected the stress is increased by the discontinuity. The increase is desirable for a worst case approximation assuming welding is not correct or of the best quality. Spring boundary conditions are also left on the original nodes after mesh refinement. This creates free nodes between the original spring locations. No additional spring elements are used in an effort to resemble irregular surface conditions on the bearing surface of the ring perimeter. Nodal constraints are also left the same after mesh refinement. This leaves a free node between the original nodes that were fixed representing a poor weld at the plug weld locations.

Reporting of Results

Stress is determined at eight locations where the stress is highest in that quadrant of the ring and reported in pounds per square inch. Locations are designated at the top, bottom, front, and back of the inner and outer radius of the ring (see figure 21 and 10). The highest stress of the two highlighted plates in figure 21 is sampled. The maximum principal stress is taken at the centroid of the plate to avoid major stress concentration effects. The stress is reported by the software for the top, bottom, and middle surface of the plate. The maximum stress recorded is regardless of the surface on which it acts. The maximum absolute value of the principle stress at the front and back locations is used to find the angle in the spreadsheet model for the axial effective section. The stress recorded at the top and bottom is used to find the angle in the spreadsheet for the bending effective section. Recorded plate principal stress is given in Table 1. Note that some cases only contain two rings.

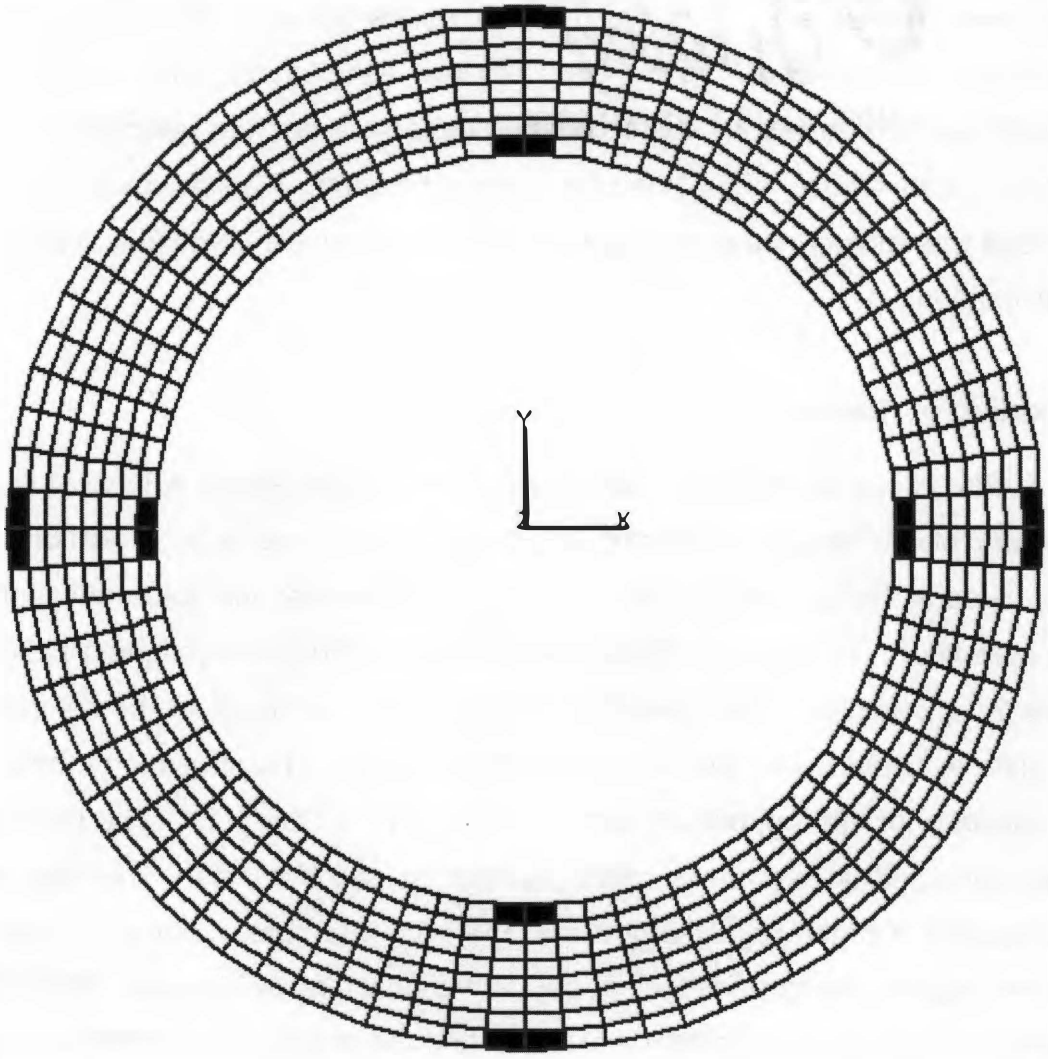

Figure 21 – Plate Sampling Locations

Table 1 – Recorded Principal Stress Data

		Front		Back		Top		Bottom	
Case	Ring	Inside	Outside	Inside	Outside	Inside	Outside	Inside	Outside
1	Top	-1900	-2058	39008	13918	-678	-1642	-678	670
	Middle								
	Bottom	10787	26963	-1301	-1430	-2180	2583	-2290	2583
2	Top	1367	876	-6442	5278	-3159	3071	-3386	3071
	Middle								
	Bottom	1732	12196	-829	-555	-1222	1049	-1222	1049
3	Top	1297	839	-6917	4408	-3212	3261	-3451	3264
	Middle								
	Bottom	-2428	12329	-787	-555	-1025	890	-1024	890
4	Top	-2290	-2682	47914	22694	-1852	1214	-1936	-1721
	Middle	4309	-2782	9987	-18088	-2594	3113	-5514	3950
	Bottom	10687	-19285	-1482	-1152	-1493	-2771	-1863	2431
5	Top	4396	3035	6786	9091	-5040	-3935	-6703	-4289
	Middle	1795	780	-2535	9142	2257	2011	2127	3677
	Bottom	-1938	-6838	-234	-83	1070	-974	-918	-676
6	Top	-2132	-1925	18043	21128	-3404	-2533	-3140	-3962
	Middle	4479	-3814	-3394	-14417	-3790	4537	-5029	4796
	Bottom	2745	13920	-685	-480	-1399	-1271	-1399	-1271
7	Top	-2437	-4138	25275	25706	-5817	5919	-4768	5919
	Middle								
	Bottom	19241	27368	-3427	-2909	-5317	7698	-6234	7698
8	Top	-2328	-5616	25900	21876	-4964	4436	-3223	-4478
	Middle								
	Bottom	16695	24441	-2434	-2776	-5309	-4820	-5717	6339
9	Top	-1931	-2666	22333	17269	-2719	2286	-2260	2286
	Middle								
	Bottom	12068	22000	-1660	-1829	-2669	4040	-2669	4040
10	Top	-3307	-5724	22219	22469	-7920	8284	-6391	-7311
	Middle	4614	2879	7306	-5628	3980	6209	3663	11151
	Bottom	20684	29298	-2747	-3061	-3914	-5323	-5580	4910
11	Top	-3273	-5638	20568	20326	-7335	8053	-6193	8053
	Middle	4985	2914	-4865	-3784	5046	7645	4445	13519
	Bottom	16752	25025	-2157	-2339	-3640	-10654	-4332	5298
12	Top	-3456	-6050	19105	17917	-8422	8949	-6774	-18859
	Middle	5966	4047	-5102	-3152	7779	11245	6540	19452
	Bottom	11830	20426	-1242	-1381	-2015	3063	-2015	3063
13	Top	-3443	-5938	21886	25973	-6045	7888	-6045	7888
	Middle								
	Bottom	25964	27035	-3795	-4842	-7110	9917	25964	27304
14	Top	-2437	-4138	25275	25706	-5817	5919	-4768	5919
	Middle								
	Bottom	19241	27368	-3427	-2909	-5317	7698	-6234	7698
15	Top	-1479	-2436	12874	24647	-4190	4075	-3871	-8562
	Middle								
	Bottom	7712	27141	-2312	-2154	-3838	5458	-4209	5458

Table 1. Continued.

		Front		Back		Top		Bottom	
Case	Ring	Inside	Outside	Inside	Outside	Inside	Outside	Inside	Outside
16	Top	-4511	-7837	23353	18896	-9311	10763	-7774	-8677
	Middle	6620	4749	-6283	-7335	9042	13206	7032	10059
	Bottom	17206	19947	-1543	-1957	-2841	3976	-2841	3976
17	Top	-3456	-6050	19105	17917	-8422	11245	-6774	-18859
	Middle	5966	4047	-5102	-3152	7779	3063	6540	19452
	Bottom	11830	20426	-1242	-1381	-2015	7888	-2015	3063
18	Top	-2376	-4185	10669	17202	-6182	6870	-5573	-5573
	Middle	5053	3220	-3677	-2420	5493	15311	5248	5248
	Bottom	4078	20038	-944	-876	-1600	2259	-1649	-1649
19	Top	-5527	-10125	21926	18637	-8080	9908	-8080	-8080
	Middle								
	Bottom	17377	18005	-4242	-6491	-8343	10043	-8323	10043
20	Top	-3974	-6418	21358	17910	-6418	7626	-6418	-6418
	Middle								
	Bottom	16973	18278	-3411	-4735	-6470	7773	-6470	-6470
21	Top	-2307	-4634	16378	17045	-4698	5284	-4698	-4698
	Middle								
	Bottom	11900	18800	-2559	-2975	-4553	5478	-4553	-4553
22	Top	-5253	-8501	50897	141537	11896	76280	11896	11896
	Middle								
	Bottom	27342	-134457	-7729	-12070	7034	42741	12674	42741
23	Top	-3762	-5641	-19855	105841	7689	55924	7689	55924
	Middle								
	Bottom	-7054	-98139	-6386	-8953	4612	29270	4612	4612
24	Top	-2208	-1261	6843	62235	4613	36716	4613	4613
	Middle								
	Bottom	-3934	-52347	-5053	-6214	2642	17432	2642	17432
25	Top	-2703	-4310	12569	19592	-5678	5919	-5678	5919
	Middle								
	Bottom	8565	20888	-2980	-2843	-4312	5556	-4312	5556
26	Top	-2547	-4098	11909	17651	-5098	5331	-5098	5331
	Middle								
	Bottom	7810	19575	-2650	-2532	-3859	4970	-3859	4970
27	Top	-2453	-3950	11506	16274	-4602	4828	-4602	4828
	Middle								
	Bottom	7063	18601	-2391	-2280	-3519	4535	-3519	4535

Chapter Four

Statistical Analysis

Multivariate Regression

If the spreadsheet model took into account everything that affects the stress in the rings then, the angle that determines section width would be the same for every model created. This also assumes that the finite element model used to determine the angle is exactly correct. Unfortunately this is not the case, so some type of approximation is needed to account for neglected effects.

Statistical software can determine what variables will bring about a better estimation of the section angle by using multivariate regression. All the variables used to create the spreadsheet model are entered into the statistical modeling platform to obtain the probability of the variables effect on the angle estimation. These variables are listed in Table 2 located in Chapter 5. Multiple combinations of the variables are also checked. The software allows multiplication of the variables by one another, i.e. ring depth times ring thickness. The variables squared and cubed are also entered and checked for effect. The type of fit used to approximate the angle is linear and derived as follows,

$$\theta = b + V_1 \cdot P_1 + V_2 \cdot P_2 + ... + V_n \cdot P_n \qquad \text{(Equation 17)}$$

where Pn is the parameter estimate, Vn is the variable, and b is the intercept.

Final Model Assembly

The parameter estimates and intercept generated by the statistics software to approximate the angle are entered into the spreadsheet model. A new stress is calculated based on the approximation. This stress is then compared to the actual stress determined by the finite element model. The

actual and approximate angle can also be compared. Percent differences are calculated between the actual and approximate stresses to determine what additional factors of safety should be used in design of the rings.

Chapter Five

Results and Conclusions

Overall Results

In almost all of the cases the ring with the highest stress was either the top or bottom ring. The middle ring contained the highest stress in case 5 but only by .051 ksi. The maximum stress was always found to be on either the top or bottom surface of the ring and at either the inner or outer radius of the ring. Figure 22 shows the typical stress distribution in the top surface of the top and bottom rings and Figure 23 shows that of the bottom surface. It is evident that the majority of the stress in the top ring travels through the sections of the ring with the most constraint by comparing to the boundary condition locations (see Figure 24). This is typical of all cases and was expected. The same effect is true for the bottom ring where the majority of the stress also develops in the part of the ring closest to the location of the plug weld. These effects reveal that only

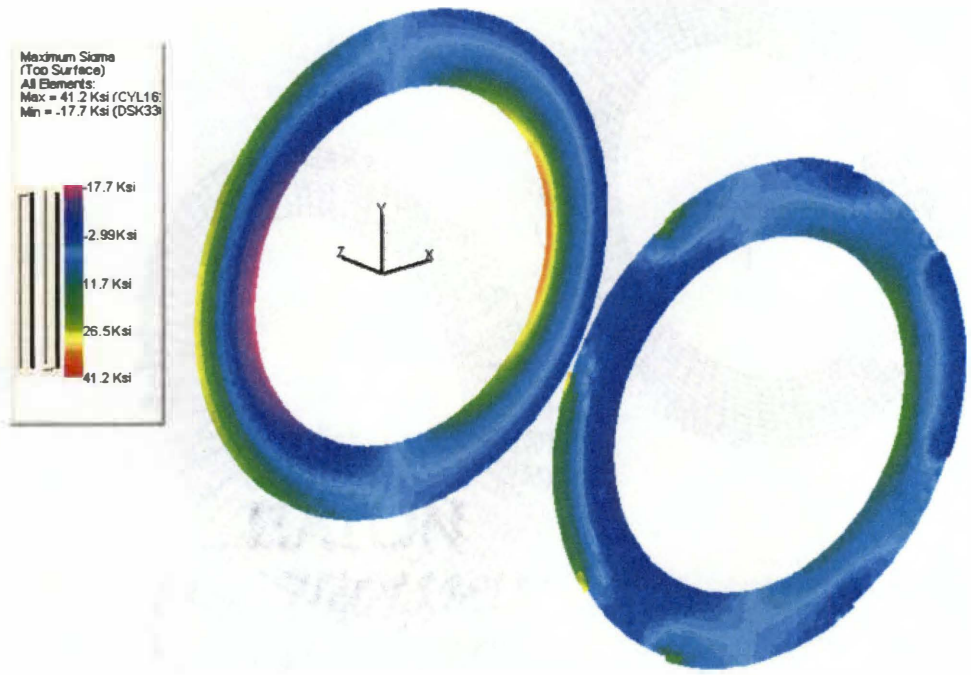

Figure 22 – Top Surface Ring Stress

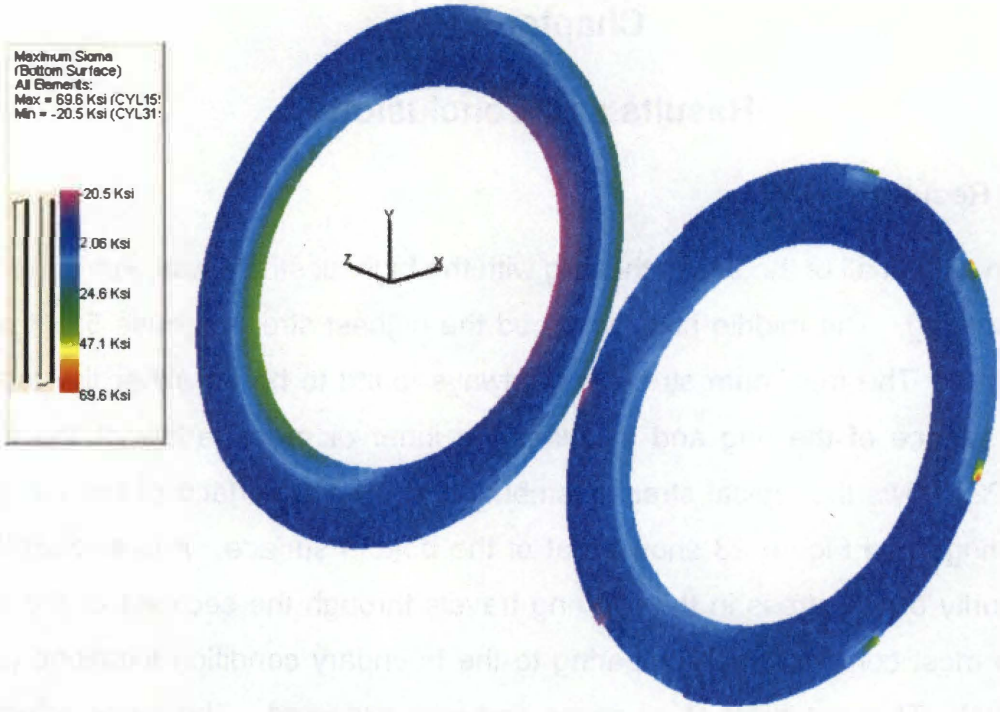

Figure 23 – Bottom Surface Ring Stress

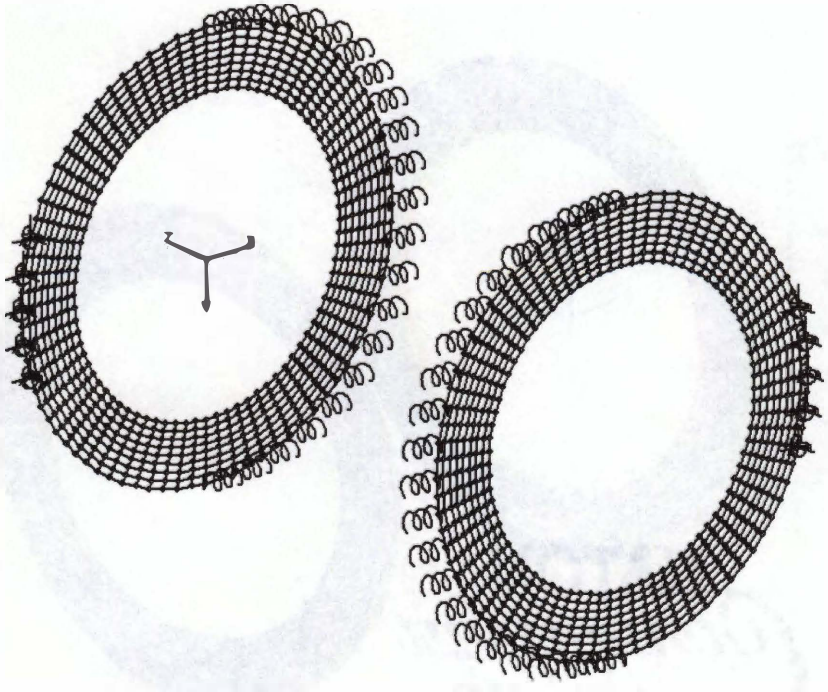

Figure 24 – Ring Boundary Conditions

the axial components of the models will contain the maximum stress. Stress concentrations can also be seen on the bottom ring in figure 23 where the plug weld terminates.

By examining the deflection of the ring some insight into the effects of the lateral load can be gained. Figure 25 is a cross-section of a two ring system in the x-z plane where the highest stress is found. The column deflection is superimposed for reference. Deflection of the inside radius of the rings exhibits both positive translation in the x-direction with rotation about some point interior to the inside radius. Rotation and deflection in the bottom ring are much less than those of the top ring. This seems logical since the top ring is encountered first in the path of the load. It is also interesting to note that the deflection is not symmetrical about the z-axis in either ring.

Results by Case

The results for each case are listed in Table 2 along with the pertinent variables used to define each case. For cases 1, 2, and 3 two rings are used and the spacing between each ring varies. Stress in the bottom ring is 30.7 ksi,

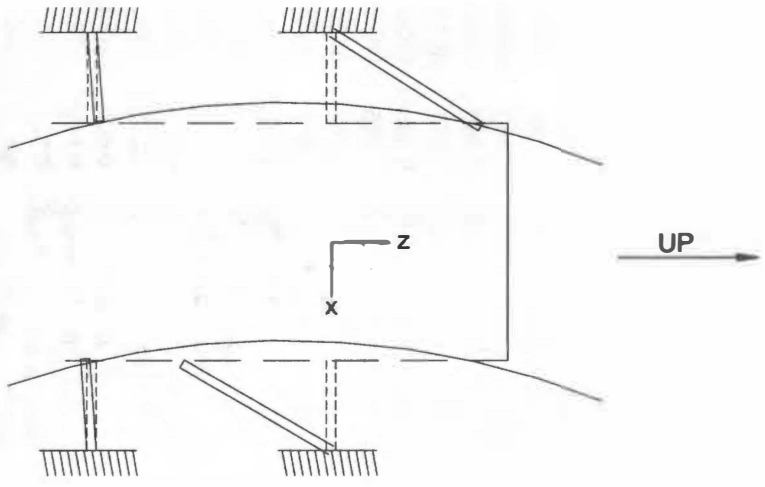

Figure 25 – Typical Ring Deflection

Table 2 - Actual Stress by Case

Case #	O pipe dia	O pipe wall	In pipe dia	IN pipe wall	Force	Moment arm (in)	t cap ring	t middle ring	t bottom ring	cap to ring dist	ring to ring dist	Cap eff design angle	Middle eff design angle	Bottom eff design angle
1	6.625	0.280	4.000	0.226	691	96.000	0.375	0.000	0.375	5.000	5.000	5.162		5.132
2	6.625	0.280	4.000	0.226	691	96.000	0.375	0.000	0.375	6.000	6.000	15.211		10.090
3	6.625	0.280	4.000	0.226	691	96.000	0.375	0.000	0.375	7.000	7.000	15.628		5.982
4	6.625	0.280	4.000	0.226	691	96.000	0.375	0.375	0.375	4.000	6.000	3.047	2.802	7.289
5	6.625	0.280	4.000	0.226	691	96.000	0.375	0.375	0.375	4.000	8.000	9.298	3.485	12.760
6	6.625	0.280	4.000	0.226	691	96.000	0.375	0.375	0.375	4.000	10.000	5.917	4.131	9.166
7	16.000	0.500	10.750	0.365	8635	96.000	0.500	0.000	0.500	8.000	8.000	12.285		10.255
8	16.000	0.500	10.750	0.365	8635	96.000	0.500	0.000	0.500	10.000	10.000	9.091		9.093
9	16.000	0.500	10.750	0.365	8635	96.000	0.500	0.000	0.500	16.000	16.000	8.571		7.301
10	16.000	0.500	10.750	0.365	8635	96.000	0.500	0.500	0.500	4.000	12.000	12.886	16.331	11.483
11	16.000	0.500	10.750	0.365	8635	96.000	0.500	0.500	0.500	4.000	16.000	8.804	16.986	9.818
12	16.000	0.500	10.750	0.365	8635	96.000	0.500	0.500	0.500	4.000	28.000	5.620	11.653	6.518
13	16.000	0.500	10.750	0.365	8635	96.000	0.375	0.000	0.375	8.000	8.000	14.244		13.065
7	16.000	0.500	10.750	0.365	8635	96.000	0.500	0.000	0.500	8.000	8.000	12.285		10.255
15	16.000	0.500	10.750	0.365	8635	96.000	0.750	0.000	0.750	8.000	8.000	9.966		7.340
16	16.000	0.500	10.750	0.365	8635	96.000	0.375	0.375	0.375	4.000	28.000	6.884	11.653	8.738
12	16.000	0.500	10.750	0.365	8635	96.000	0.500	0.500	0.500	4.000	28.000	5.620	11.653	6.518
18	16.000	0.500	10.750	0.365	8635	96.000	0.750	0.750	0.750	4.000	28.000	4.894	11.653	4.845
19	28.000	0.625	18.000	0.500	33789	96.000	0.375	0.000	0.375	14.000	14.000	21.452		19.895
20	28.000	0.625	18.000	0.500	33789	96.000	0.500	0.000	0.500	14.000	14.000	19.493		17.085
21	28.000	0.625	18.000	0.500	33789	96.000	0.750	0.000	0.750	14.000	14.000	17.174		14.169
22	36.000	0.500	32.000	0.688	149657	96.000	0.750	0.000	0.750	24.000	24.000	4.014		3.183
23	36.000	0.500	32.000	0.688	149657	96.000	1.000	0.000	1.000	24.000	24.000	3.830		3.874
24	36.000	0.500	32.000	0.688	149657	96.000	1.500	0.000	1.500	38.000	38.000	3.637		3.325
25	36.000	0.500	24.000	0.500	61344	96.000	1.000	0.000	1.000	16.000	16.000	13.499		11.381
26	36.000	0.500	24.000	0.500	61344	96.000	1.000	0.000	1.000	18.000	18.000	15.457		10.767
27	36.000	0.500	24.000	0.500	61344	96.000	1.000	0.000	1.000	20.000	20.000	13.569		10.190

15.5 ksi, and 12.3 ksi for ring spacings of 10 in., 12 in., and 14 in. respectively. Stress in the bottom ring of these cases reacted as expected with the stress dropping as the distance between the rings increased. Stress in the top ring dropped sharply between case 1 and 2 from 39 ksi to 6.4 ksi then increased slightly to 6.9 ksi for case 3.

Cases 4, 5, and 6 are identical to cases 1, 2, and 3 respectively with the exception of an additional ring located 4 in. below the top ring. The stress dropped with the addition of the middle ring from 30.7 ksi to 19.3 ksi between case 1 and 4 and from 15.5 ksi to 6.8 ksi for case 2 and 5 (see figure 26). The stress for case 3 increased slightly from 12.3 ksi to 13.9 ksi. Stress in the top ring increased from 39 ksi to 47.9 ksi between case 1 and 4, from 6.4 ksi to 9.1 ksi between case 2 and 5, and from 6.9 ksi to 21.1 ksi between case 3 and 6. Stress in the middle ring is lower than the other two rings for case 4. In case 5 the middle ring stress is higher than the top and bottom rings, but only slightly

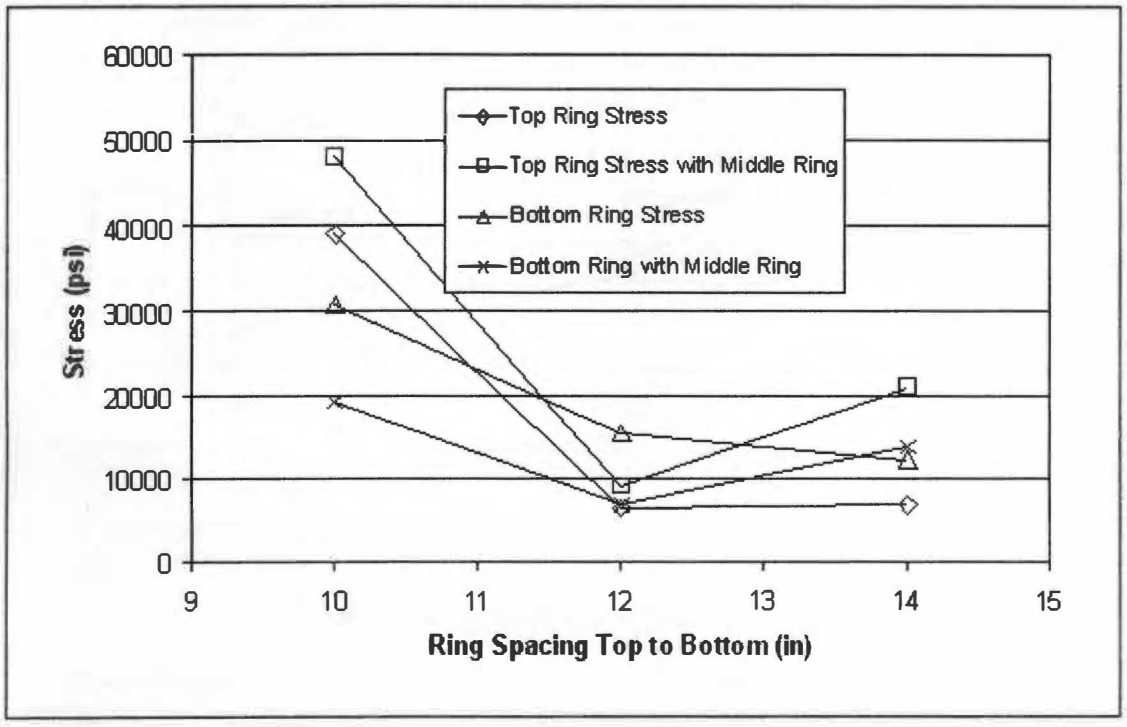

Figure 26 –Stress for Case 1 to 6

above that of the top ring. Middle ring stress is in-between the top and bottom rings in case 6.

In cases 7, 8, and 9 larger columns, ring thickness, and ring spacing are used than in the first 3 cases without a middle ring. Stresses in the bottom ring are 27.4 ksi, 24.4 ksi and 22 ksi for case 7, 8, and 9 respectively. This decrease in stress as the spacing between the rings increased is the expected result. In the top ring stresses are 25.7 ksi, 25.9 ksi, and 22.3 ksi for cases 7, 8, and 9 respectively. Here the stress peaked with the rings spaced at 20 in., but only by a small amount.

Cases 10, 11, and 12 are the same as cases 7, 8, and 9 with the exception that middle rings are added. Stresses in the bottom ring are 29.3 ksi, 25 ksi, and 20.4 ksi for case 10, 11, and 12 respectively (see figure 27). Stress in the bottom ring is higher with the addition of the middle ring in cases 10 and 11 and only slightly lower in case 12. Stresses in the top ring are 22.5 ksi, 20.6 ksi

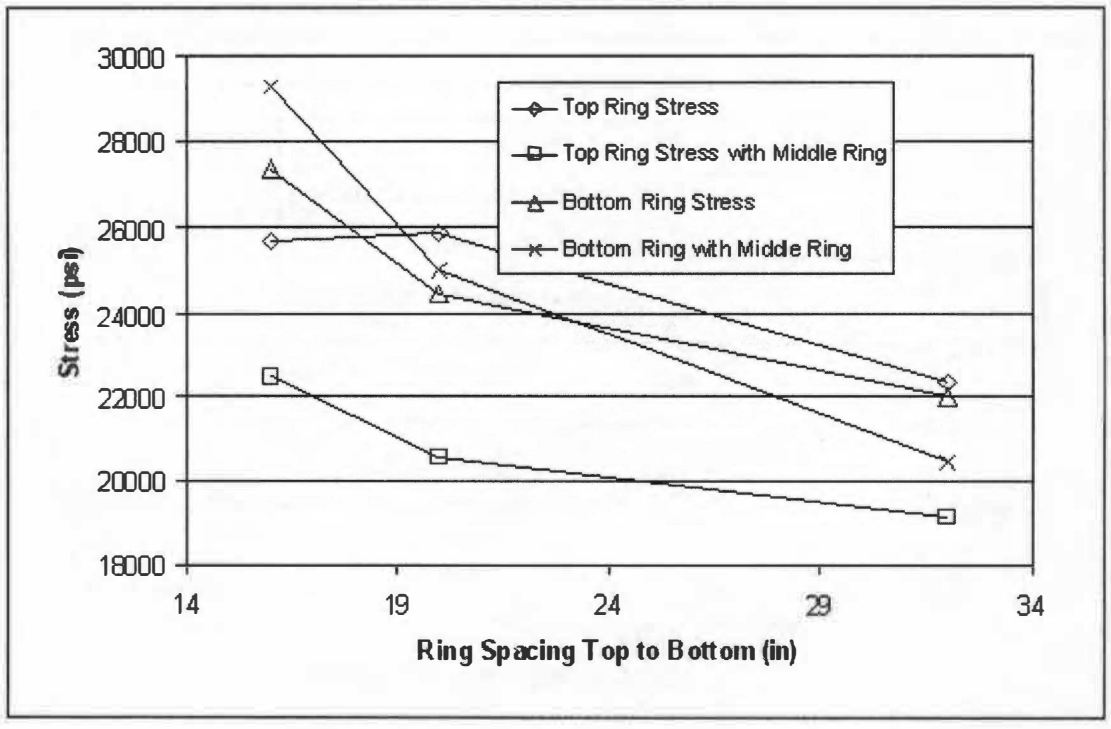

Figure 27 – Stress for Case 7 to 12

and 19.1 ksi for case 10, 11, and 12 respectively. Stress in the cap ring is lowered by the introduction of a middle ring. In both the top and bottom rings the stress decreased as the distance between the rings increased. Stress in the middle ring is much lower than that of the top and bottom rings. The middle ring stress edged slightly higher with rings at 32" between the top and bottom rings after dropping with the rings at 20".

Cases 13, 14, and 15 have the same configuration as cases 7, 8, and 9 with the exception of the distances between the rings are held to 16" and the rings increase in thickness. The stress in the cap plate decreases as the thickness of the rings increase, but only by a small amount. Stress in the bottom ring has no significant change in stress due to difference in ring thickness. These two effects were not expected. Overall stress in the cap ring is approximately 2 ksi less than the stress in the bottom ring.

Cases 16, 17, and 18 are the same as cases 13, 14, and 15 respectively with the exception of a middle ring is added and the spacing is held at 32" from top to bottom ring. The stress in the bottom ring again had only minimal change as with the previous three cases and had a magnitude of around 20 ksi. Stress in the top ring is 23.3 ksi, 19.1 ksi, and 17.2 ksi for cases 16, 17, and 18 respectively (see figure 28). The top stress has a more substantial decrease with increasing thickness in these three cases than in cases 13, 14, and 15. Stress in the middle ring also shows significant decrease with increasing thickness. The magnitude of stress in the top and bottom rings is much greater than that of the middle ring.

In cases 19, 20, and 21 the top and bottom column size is increased and the cap to bottom ring distance is held to 28 in. Only two rings are used and the ring depth is much larger than in any previous case. Ring thickness is increased for each successive case. Although the moment in the top column is larger compared to the moment in cases 13, 14, and 15, the stress is lower with the same thickness rings for both the top and bottom rings (see figure 29). Stress in

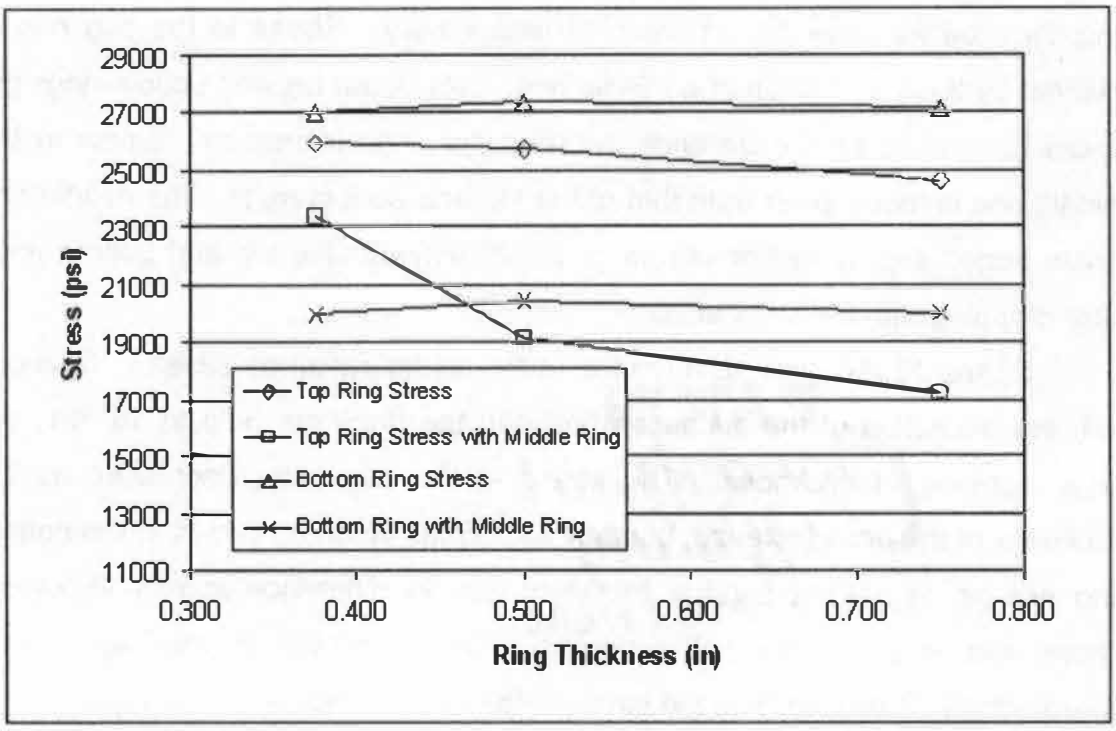

Figure 28 – Stress for Case 13 to 18

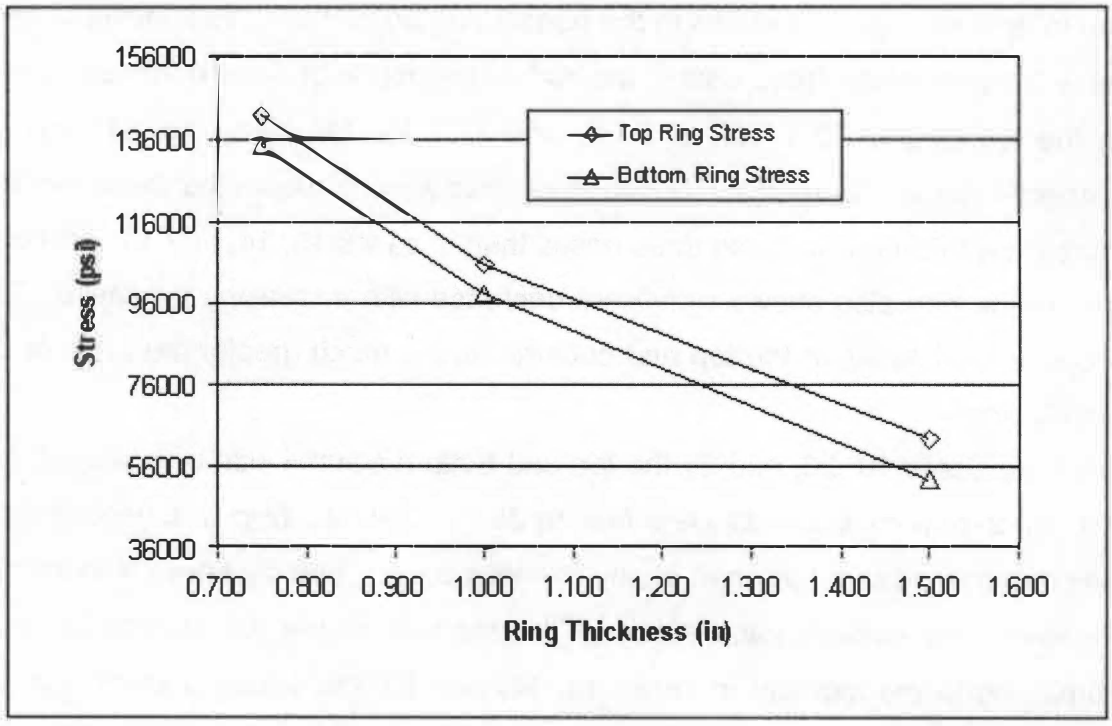

Figure 29 – Stress for Case 19 to 21

the bottom ring slightly increased with increasing thickness. Stress in the top ring decreased significantly as the ring thickness increased.

The configuration of cases 22, 23, and 24 is special in that the ring depth is small in relation to the column diameter. Here both the cap to ring distance and ring thickness is varied. A definite reduction in the amount of stress is observed as the distance and thickness are increased (see figure 30).

The final cases 25, 26, and 27 are similar to the previous cases except that the top column is smaller and the ring thickness is held constant as the distance between the rings is increased. Stress in both top and bottom rings behaved as expected and decreased as the distance between rings increased (see figure 31). In all three cases the magnitude of the stress in the bottom ring is greater than the stress in the top ring.

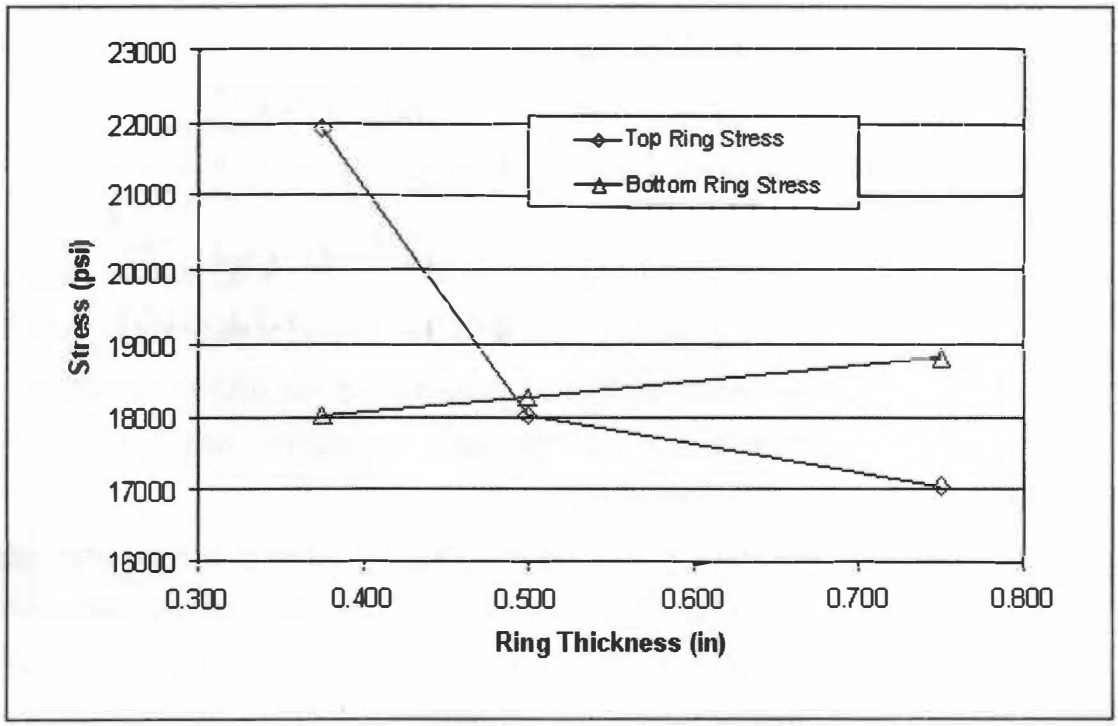

Figure 30 – Stress for Case 22 to 24

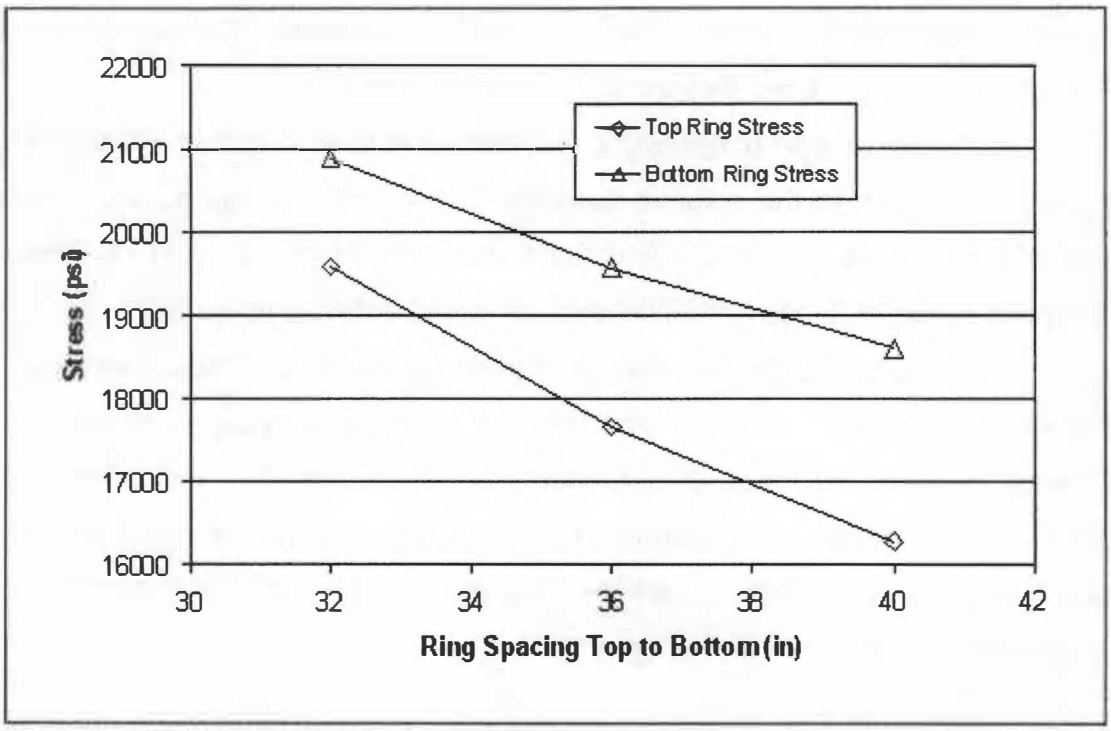

Figure 31 – Stress for Case 25 to 27

Statistical Results

The angle used in determining section width was anticipated to have the same value for every configuration, assuming the spreadsheet model took into account every effect the variables have on determining the stress. By examining Table 3 it is evident that this is not the case and further leverage from the variables is required by statistical modeling.

By examining the first three cases with respect to the larger column cases it is found that the inertia of the top column has a large effect on the stress when the column is less rigid. Column rigidity is the basis of the spreadsheet model and its effects are needed in determining the stress.

The effective top angle, variables, and inertia calculation are entered in the statistical modeling platform and an approximation is attempted. The probability that inertia has an effect on the angle is greater than the probability of

Table 3 - Effective Design Angle

Case #	O pipe dia	O pipe wall	In pipe dia	IN pipe wall	Force	Moment arm (in)	t cap ring	t middle ring	t bottom ring	cap to ring dist	ring to ring dist	Cap eff design angle	Middle eff design angle	Bottom eff design angle
1	6.625	0.280	4.000	0.226	691	96.000	0.375	0.000	0.375	5.000	5.000	5.162		5.132
2	6.625	0.280	4.000	0.226	691	96.000	0.375	0.000	0.375	6.000	6.000	15.211		10.090
3	6.625	0.280	4.000	0.226	691	96.000	0.375	0.000	0.375	7.000	7.000	15.628		5.982
4	6.625	0.280	4.000	0.226	691	96.000	0.375	0.375	0.375	4.000	6.000	3.047	2.802	7.289
5	6.625	0.280	4.000	0.226	691	96.000	0.375	0.375	0.375	4.000	8.000	9.298	3.485	12.760
6	6.625	0.280	4.000	0.226	691	96.000	0.375	0.375	0.375	4.000	10.000	5.917	4.131	9.166
7	16.000	0.500	10.750	0.365	8635	96.000	0.500	0.000	0.500	8.000	8.000	12.285		10.255
8	16.000	0.500	10.750	0.365	8635	96.000	0.500	0.000	0.500	10.000	10.000	9.091		9.093
9	16.000	0.500	10.750	0.365	8635	96.000	0.500	0.000	0.500	16.000	16.000	8.571		7.301
10	16.000	0.500	10.750	0.365	8635	96.000	0.500	0.500	0.500	4.000	12.000	12.886	16.331	11.483
11	16.000	0.500	10.750	0.365	8635	96.000	0.500	0.500	0.500	4.000	16.000	8.804	16.986	9.818
12	16.000	0.500	10.750	0.365	8635	96.000	0.500	0.500	0.500	4.000	28.000	5.620	11.653	6.518
13	16.000	0.500	10.750	0.365	8635	96.000	0.375	0.000	0.375	8.000	8.000	14.244		13.065
7	16.000	0.500	10.750	0.365	8635	96.000	0.500	0.000	0.500	8.000	8.000	12.285		10.255
15	16.000	0.500	10.750	0.365	8635	96.000	0.750	0.000	0.750	8.000	8.000	9.966		7.340
16	16.000	0.500	10.750	0.365	8635	96.000	0.375	0.375	0.375	4.000	28.000	6.884	11.653	8.738
12	16.000	0.500	10.750	0.365	8635	96.000	0.500	0.500	0.500	4.000	28.000	5.620	11.653	6.518
18	16.000	0.500	10.750	0.365	8635	96.000	0.750	0.750	0.750	4.000	28.000	4.894	11.653	4.845
19	28.000	0.625	18.000	0.500	33789	96.000	0.375	0.000	0.375	14.000	14.000	21.452		19.895
20	28.000	0.625	18.000	0.500	33789	96.000	0.500	0.000	0.500	14.000	14.000	19.493		17.085
21	28.000	0.625	18.000	0.500	33789	96.000	0.750	0.000	0.750	14.000	14.000	17.174		14.169
22	36.000	0.500	32.000	0.688	149657	96.000	0.750	0.000	0.750	24.000	24.000	4.014		3.183
23	36.000	0.500	32.000	0.688	149657	96.000	1.000	0.000	1.000	24.000	24.000	3.830		3.874
24	36.000	0.500	32.000	0.688	149657	96.000	1.500	0.000	1.500	38.000	38.000	3.637		3.325
25	36.000	0.500	24.000	0.500	61344	96.000	1.000	0.000	1.000	16.000	16.000	13.499		11.381
26	36.000	0.500	24.000	0.500	61344	96.000	1.000	0.000	1.000	18.000	18.000	15.457		10.767
27	36.000	0.500	24.000	0.500	61344	96.000	1.000	0.000	1.000	20.000	20.000	13.569		10.190

effect of any other variable for the cap and middle rings (see figures 32, 33, and 34). The values for the probability > |t| of inertia are .0003, .0641, and .0052 for the cap, bottom, and middle rings respectively where the higher the probability of effect when the number is lower. The idea that column rigidity is a major effect is confirmed by these numbers. The variable with the most probability of effect in the bottom ring model is the distance between the top and bottom rings. For this variable the probability of effect is .0291.

The correlations for the angle estimates are .97, .98, and .94 for the top, middle, and bottom rings respectively. The number of variables used for the top and bottom fit were large in comparison with that of the middle ring. Distance between the rings has the greatest effect on the stress in the rings. This result was expected. When the inertia of the top column is not significant enough to introduce adequate rigidity into the model the distance between the rings will have varying effects.

Actual to Estimated Comparison

With the spreadsheet model modified to take into account additional variable effects, the actual to estimated results can be compared (see Table 4). The average percent differences between the actual to the estimated are 9.2, 12.7, and 9.2 for the cap, middle, and bottom rings respectively. The maximum percent differences are 31.1, 41.4, and 39.1 and occur in cases 5, 5, and 3 for the same respective rings.

The final spreadsheet model modified to take into account the variable effects allows many configurations to be analyzed. Being that the model is in spreadsheet form makes the analysis much quicker than if finite elements were used for every design. Allowances are needed on smaller columns due to the high percent difference between the actual and approximate, but the majority of designs need only an additional 10 percent reduction in the allowable stress.

Response Angle cap

Actual by Predicted Plot

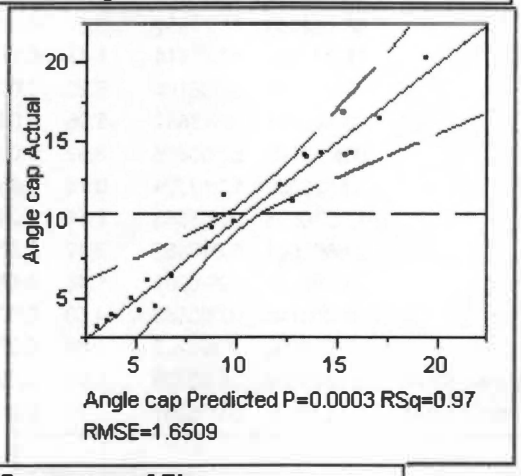

Summary of Fit

RSquare	0.968708
RSquare Adj	0.906125
Root Mean Square Error	1.650886
Mean of Response	10.41172
Observations (or Sum Wgts)	25

Analysis of Variance

Source	DF	Sum of Squares	Mean Square	F Ratio
Model	16	674.97410	42.1859	15.4787
Error	8	21.80339	2.7254	Prob > F
C. Total	24	696.77749		0.0003

Figure 32 – Cap Ring Statistical Results

Parameter Estimates

Term	Estimate	Std Error	t Ratio	Prob>|t|
Intercept	-769.0841	186.4892	-4.12	0.0033
I top	-0.316738	0.053128	-5.96	0.0003
New moment kip ft	-1.286489	0.998776	-1.29	0.2337
cap to ring dist	88.82509	18.19497	4.88	0.0012
ring to ring dist	98.664986	18.71551	5.27	0.0008
Ring diff	71.036041	48.23614	1.47	0.1791
Ring dist cub	0.042792	0.008101	5.28	0.0007
Ring dist sqr	-3.442451	0.653841	-5.26	0.0008
M sqr	0.0029189	0.000806	3.62	0.0067
mid t sqr	2.1525052	12.12384	0.18	0.8635
cap t sq	17.076935	15.3583	1.11	0.2985
Ring t sum	3.6801801	8.818455	0.42	0.6874
t cap ring	-37.98039	26.0991	-1.46	0.1837
(Ring diff-2.46292)*(Ring dist cub-41753.6)	-0.003748	0.000833	-4.50	0.0020
(Ring dist sqr-938.24)*(M sqr-211596)	-0.000002	4.885e-7	-4.89	0.0012
(New moment kip ft-263.957)*(ring to ring dist-15.44)	0.1874518	0.03735	5.02	0.0010
(New moment kip ft-263.957)*(cap to ring dist-11.28)	0.1346801	0.035281	3.82	0.0051

Effect Tests

Source	Nparm	DF	Sum of Squares	F Ratio	Prob > F
I top	1	1	96.870881	35.5434	0.0003
New moment kip ft	1	1	4.521786	1.6591	0.2337
cap to ring dist	1	1	64.953513	23.8324	0.0012
ring to ring dist	1	1	75.745499	27.7922	0.0008
Ring diff	1	1	5.910802	2.1688	0.1791
Ring dist cub	1	1	76.051524	27.9045	0.0007
Ring dist sqr	1	1	75.548313	27.7198	0.0008
M sqr	1	1	35.783561	13.1295	0.0067
mid t sqr	1	1	0.085910	0.0315	0.8635
cap t sq	1	1	3.369516	1.2363	0.2985
Ring t sum	1	1	0.474665	0.1742	0.6874
t cap ring	1	1	5.771672	2.1177	0.1837
Ring diff*Ring dist cub	1	1	55.220367	20.2612	0.0020
Ring dist sqr*M sqr	1	1	65.059028	23.8712	0.0012
New moment kip ft*ring to ring dist	1	1	68.650419	25.1889	0.0010
New moment kip ft*cap to ring dist	1	1	39.714399	14.5718	0.0051

Figure 32. Continued.

Response bottom angle

Actual by Predicted Plot

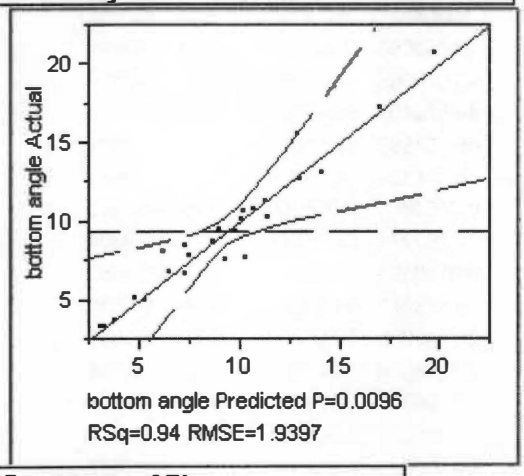

Summary of Fit

RSquare	0.938947
RSquare Adj	0.790675
Root Mean Square Error	1.939655
Mean of Response	9.36636
Observations (or Sum Wgts)	25

Analysis of Variance

Source	DF	Sum of Squares	Mean Square	F Ratio
Model	17	405.02391	23.8249	6.3326
Error	7	26.33582	3.7623	Prob > F
C. Total	24	431.35974		0.0096

Figure 33 – Bottom Ring Statistical Results

Parameter Estimates

Term	Estimate	Std Error	t Ratio	Prob>|t|
Intercept	-649.4421	267.4369	-2.43	0.0455
I top	-0.753068	0.342892	-2.20	0.0641
New moment kip ft	-9.870065	4.202998	-2.35	0.0512
cap to ring dist	44.574409	16.53461	2.70	0.0308
ring to ring dist	45.154593	16.50015	2.74	0.0291
Ring diff	477.1338	203.9929	2.34	0.0519
Ring dist cub	0.0464863	0.017204	2.70	0.0305
Ring dist sqr	-2.692274	0.994879	-2.71	0.0304
M sqr	0.0130565	0.005791	2.25	0.0588
mid t sqr	0.673879	14.32081	0.05	0.9638
cap t sq	28.849098	18.05209	1.60	0.1541
Ring t sum	4.1286314	10.47613	0.39	0.7052
t cap ring	-55.98058	30.76567	-1.82	0.1116
Ring diff x ring dist cub	-0.003077	0.001197	-2.57	0.0370
Ring dist sqr*M sqr	-0.000005	0.000002	-2.27	0.0577
kip ft x cap to ring	0.2019148	0.07804	2.59	0.0361
Kip ftX ring to ring	0.1898777	0.076826	2.47	0.0427
M sqr x ring dist cub	2.8698e-8	1.56e-8	1.84	0.1085

Effect Tests

Source	Nparm	DF	Sum of Squares	F Ratio	Prob > F
I top	1	1	18.146941	4.8234	0.0641
New moment kip ft	1	1	20.747733	5.5147	0.0512
cap to ring dist	1	1	27.342119	7.2675	0.0308
ring to ring dist	1	1	28.175855	7.4891	0.0291
Ring diff	1	1	20.582555	5.4708	0.0519
Ring dist cub	1	1	27.469552	7.3013	0.0305
Ring dist sqr	1	1	27.551635	7.3232	0.0304
M sqr	1	1	19.126762	5.0838	0.0588
mid t sqr	1	1	0.008331	0.0022	0.9638
cap t sq	1	1	9.608565	2.5539	0.1541
Ring t sum	1	1	0.584332	0.1553	0.7052
t cap ring	1	1	12.456353	3.3109	0.1116
Ring diff x ring dist cub	1	1	24.842387	6.6030	0.0370
Ring dist sqr*M sqr	1	1	19.346565	5.1423	0.0577
kip ft x cap to ring	1	1	25.185584	6.6943	0.0361
Kip ftX ring to ring	1	1	22.981847	6.1085	0.0427
M sqr x ring dist cub	1	1	12.724815	3.3822	0.1085

Figure 33. Continued.

Response middle angle

Whole Model

Actual by Predicted Plot

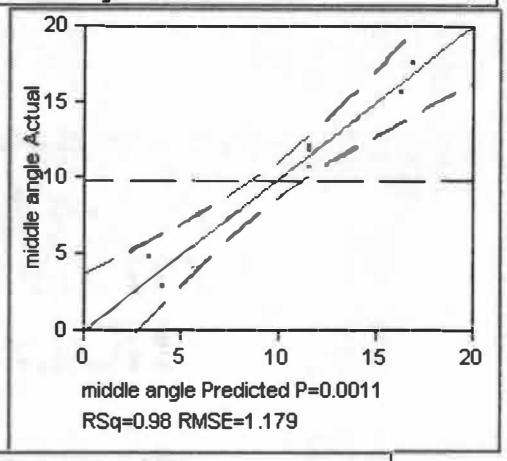

Summary of Fit

RSquare	0.975941
RSquare Adj	0.957897
Root Mean Square Error	1.179045
Mean of Response	9.836903
Observations (or Sum Wgts)	8

Analysis of Variance

Source	DF	Sum of Squares	Mean Square	F Ratio
Model	3	225.56232	75.1874	54.0860
Error	4	5.56059	1.3901	Prob > F
C. Total	7	231.12291		0.0011

Lack Of Fit

Source	DF	Sum of Squares	Mean Square	F Ratio
Lack Of Fit	2	4.2571034	2.12855	3.2659
Pure Error	2	1.3034858	0.65174	Prob > F
Total Error	4	5.5605892		0.2344
				Max RSq
				0.9944

Parameter Estimates

Term	Estimate	Std Error	t Ratio	Prob>|t|
Intercept	0.2094962	2.556813	0.08	0.9386
I top	0.0746487	0.01347	5.54	0.0052
Ring dist cub	-0.00104	0.000666	-1.56	0.1935
Ring dist sqr	0.0327532	0.025397	1.29	0.2667

Effect Tests

Source	Nparm	DF	Sum of Squares	F Ratio	Prob > F
I top	1	1	42.692301	30.7106	0.0052
Ring dist cub	1	1	3.388326	2.4374	0.1935
Ring dist sqr	1	1	2.312161	1.6632	0.2667

Figure 34 – Middle Ring Statistical Results

Table 4 - Actual to Approximate Results

	Cap		Middle		Bottom		Cap			Middle			Bottom		
Case #	actual angle	approx. angle	actual angle	approx. angle	actual angle	approx. angle	actual stress	approx. stress	% diff.	actual stress	approx. stress	% diff.	actual stress	approx. stress	% diff.
1	4.281	5.162			4.980	5.132	39008	32068	17.792				30721	29762	3.120
2	16.927	15.211			7.726	10.090	6442	7463	15.851				15456	11363	26.484
3	14.310	15.628			8.079	5.982	6917	6145	11.155				12329	17155	39.146
4	3.258	3.047	2.643	2.802	7.915	7.289	47914	51311	7.089	18088	17045	5.768	19285	21141	9.627
5	11.648	9.298	4.867	3.485	15.596	12.760	9091	11915	31.068	9142	12928	41.416	6838	8908	30.268
6	4.499	5.917	2.909	4.131	7.537	9.166	21128	15815	25.145	14417	10056	30.247	13920	11146	19.929
7	12.200	12.285			10.651	10.255	25706	25458	0.966				27368	28774	5.138
8	10.266	9.091			9.512	9.093	25900	30281	16.915				24441	25879	5.884
9	8.195	8.571			6.702	7.301	22333	21140	5.344				22000	19909	9.503
10	11.228	12.886	15.714	16.331	10.313	11.483	22469	18535	17.507	7306	6876	5.892	29298	25362	13.436
11	9.486	8.804	17.655	16.986	9.399	9.818	20568	22598	9.868	4985	5306	6.448	25025	23666	5.432
12	6.165	5.620	11.954	11.653	6.875	6.518	19105	21197	10.950	5966	6180	3.589	20426	21720	6.336
13	14.291	14.244			12.721	13.065	25973	26099	0.485				27035	26021	3.751
7	12.200	12.285			10.651	10.255	25706	25458	0.966				27368	28774	5.138
15	9.970	9.966			8.458	7.340	24647	24658	0.044				27141	32205	18.659
16	6.455	6.884	12.236	11.653	8.707	8.738	23353	21687	7.134	7335	7850	7.022	19947	19858	0.444
12	6.165	5.620	11.954	11.653	6.875	6.518	19105	21197	10.950	5966	6180	3.589	20426	21720	6.336
18	4.990	4.894	10.718	11.653	5.119	4.845	17202	17569	2.135	5053	4510	10.741	20038	21273	6.163
19	21.234	21.452			20.718	19.895	21926	21584	1.561				18005	19151	6.366
20	20.332	19.493			17.262	17.085	18005	19191	6.586				18278	18552	1.499
21	16.553	17.174			13.169	14.169	17045	16166	5.158				18800	17047	9.327
22	3.796	4.014			3.351	3.183	141537	128800	8.999				134457	145525	8.232
23	4.047	3.830			3.706	3.874	105841	116159	9.749				98139	91172	7.099
24	3.638	3.637			3.325	3.325	62235	62289	0.086				52347	52346	0.002
25	14.217	13.499			11.381	11.381	19592	21042	7.403				20888	20890	0.008
26	14.202	15.457			10.767	10.767	17651	15664	11.259				19575	19575	0.002
27	14.105	13.569			10.190	10.190	16274	17167	5.484				18601	18602	0.007
							average % diff		9.172			12.746			9.161
							max % diff		31.068			41.416			39.146

Conclusions

The effective section angle can be used to estimate the stress in splice rings. The number of equations used in determining the angle is more than expected but can be accounted for in the final analysis with the original set of independent variables used. Where the rigidity of the column is in question, caution will need to be exercised since the maximum percent difference occurs in these cases.

Distance between the rings has the greatest effect on the stress in the rings. This result was expected. When the inertia of the top column is not significant enough to introduce adequate rigidity into the model, the distance between the rings will have varying effects. It seems logical that the less rigid the beam the less load will be transferred to the middle and bottom rings.

When the distance between the top and bottom column is small, the effect of ring thickness is much greater than when the difference is larger. Ring thickness is somewhat insignificant in the more typical of cases. This result was not expected. The most stress on the rings occurs when the rings are not very deep and the columns are larger. This is due to the short distance a large load is allowed to travel. With the smaller columns the stress seems to vary greatly with different ring spacing due to lack of top column rigidity.

Future Work

This thesis is limited to the use of circular columns as the main structural members. Square columns can be extrapolated from the data found here, but a more in-depth examination would be very useful. As always, more cases can be taken into consideration with the study conducted here. Physical testing by applying strain gages on a full sized model could be an alternate method of comparison to the spreadsheet model. A three dimensional finite element

approximation with the rings and columns created as three dimensional solids could yield more accurate results especially in areas such as the welds.

Another area of study can be found in the column itself. Although not taken into consideration here, the column stress is not symmetrical at the cap plate about the z-axis as is assumed in mechanics of materials. This suggests that stress concentration factors are affecting the stress at the intersection of the column and the cap ring.

References

References

[1] Jones, Benjamin, *Engineering Sign Structures, An Introduction to Analysis and Design*, ST Publications, Inc., 1998.

[2] Campbell, Gregory A., Engineering Manager of Trisect Engineering, Personal Communication, 2001.

[3] American Institute of Steel Construction, Inc., *Manual of Steel Construction*, Eighth Edition, A.I.S.C., 1980.

[4] American Society of Civil Engineers, *Minimum Design Loads for Buildings and Other Structures ASCE 7-98*, American Society of Civil Engineers, 2000

[5] Cook, Robert D., and Young, Warren C., *Advanced Mechanics of Materials*, Second Edition, Prentice-Hall, Inc., 1999.

[6] Lindeburg, Michael R., *Mechanical Engineering Reference Manual for the PE Exam*, Tenth Edition, Professional Publications, Inc., 1998.

Appendices

Appendix A

Geometric Developments

Appendix A1

Geometric Development of Effective Section Length

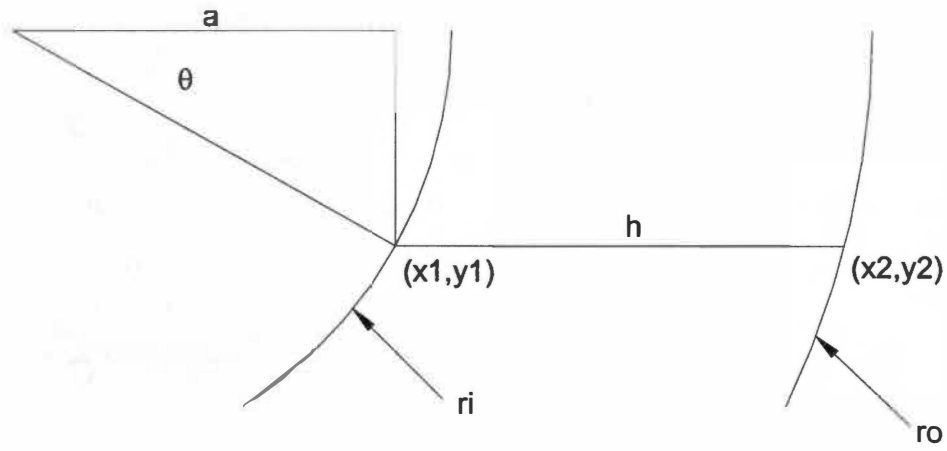

h = effective section length = x2 - x1

$a = ri \sin \theta = x1$

h = x2 - a

y2 = y1

$ri^2 = x1^2 + y1^2$

$ro^2 = x2^2 + y1^2$

$y1^2 = ro^2 - x2^2 = ri^2 - x1^2$

$x2 = (a^2 + ro^2 - ri^2)^{1/2}$

$h = (a^2 + ro^2 - ri^2)^{1/2} - a$

Appendix A2

Additional Stress from Rotation

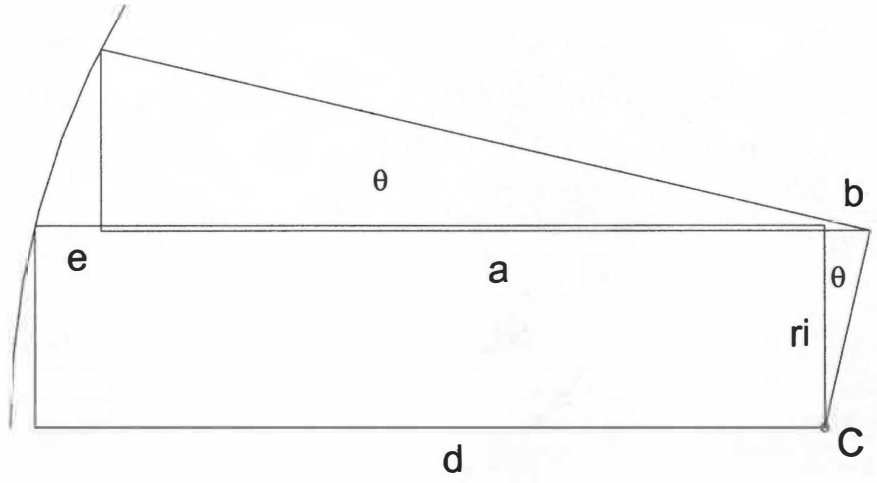

d = distance from center of rotation to ring

ri = outer radius of top column

$d + b = a + e$

$e = d + b - a$

$a = d \cos \theta$

$b = ri \tan \theta$

θ = angle of rotation of rigid beam

$e = d + ri \tan \theta - d \cos \theta$ = deflection in z-direction

$\sigma = M y / I$ = additional stress from rotation

I = Moment of Inertia about weak axis of effective section

y = half the ring thickness

$M = F h$

$F = k e$

k = stiffness of effective section in flexure

h = effective section length

Appendix B

Spreadsheet Formulas

Table 5 - Spreadsheet Formulas

Case #	O pipe dia	O pipe wall	In pipe dia	IN pipe wall	Force	Moment arm (in)	Moment (lb-in)	Ro	Ri	R diff	E
1	6.625	0.28	4	0.226	691	96	=F5*G5	=(B5/2)-C5	=D5/2	=I5-J5	29000000
2	6.625	0.28	4	0.226	691	96	=F6*G6	=(B6/2)-C6	=D6/2	=I6-J6	29000000
3	6.625	0.28	4	0.226	691	96	=F7*G7	=(B7/2)-C7	=D7/2	=I7-J7	29000000
4	6.625	0.28	4	0.226	691	96	=F8*G8	=(B8/2)-C8	=D8/2	=I8-J8	29000000
5	6.625	0.28	4	0.226	691	96	=F9*G9	=(B9/2)-C9	=D9/2	=I9-J9	29000000
6	6.625	0.28	4	0.226	691	96	=F10*G10	=(B10/2)-C10	=D10/2	=I10-J10	29000000
7	16	0.5	10.75	0.365	8635	96	=F11*G11	=(B11/2)-C11	=D11/2	=I11-J11	29000000
8	16	0.5	10.75	0.365	8635	96	=F12*G12	=(B12/2)-C12	=D12/2	=I12-J12	29000000
9	16	0.5	10.75	0.365	8635	96	=F13*G13	=(B13/2)-C13	=D13/2	=I13-J13	29000000
10	16	0.5	10.75	0.365	8635	96	=F14*G14	=(B14/2)-C14	=D14/2	=I14-J14	29000000
11	16	0.5	10.75	0.365	8635	96	=F15*G15	=(B15/2)-C15	=D15/2	=I15-J15	29000000
12	16	0.5	10.75	0.365	8635	96	=F16*G16	=(B16/2)-C16	=D16/2	=I16-J16	29000000
13	16	0.5	10.75	0.365	8635	96	=F17*G17	=(B17/2)-C17	=D17/2	=I17-J17	29000000
7	16	0.5	10.75	0.365	8635	96	=F18*G18	=(B18/2)-C18	=D18/2	=I18-J18	29000000
15	16	0.5	10.75	0.365	8635	96	=F19*G19	=(B19/2)-C19	=D19/2	=I19-J19	29000000
16	16	0.5	10.75	0.365	8635	96	=F20*G20	=(B20/2)-C20	=D20/2	=I20-J20	29000000
12	16	0.5	10.75	0.365	8635	96	=F21*G21	=(B21/2)-C21	=D21/2	=I21-J21	29000000
18	16	0.5	10.75	0.365	8635	96	=F22*G22	=(B22/2)-C22	=D22/2	=I22-J22	29000000
19	28	0.625	18	0.5	33789	96	=F23*G23	=(B23/2)-C23	=D23/2	=I23-J23	29000000
20	28	0.625	18	0.5	33789	96	=F24*G24	=(B24/2)-C24	=D24/2	=I24-J24	29000000
21	28	0.625	18	0.5	33789	96	=F25*G25	=(B25/2)-C25	=D25/2	=I25-J25	29000000
22	36	0.5	32	0.6875	149657	96	=F26*G26	=(B26/2)-C26	=D26/2	=I26-J26	29000000
23	36	0.5	32	0.6875	149657	96	=F27*G27	=(B27/2)-C27	=D27/2	=I27-J27	29000000
24	36	0.5	32	0.6875	149657	96	=F28*G28	=(B28/2)-C28	=D28/2	=I28-J28	29000000
25	36	0.5	24	0.5	61344	96	=F29*G29	=(B29/2)-C29	=D29/2	=I29-J29	29000000
26	36	0.5	24	0.5	61344	96	=F30*G30	=(B30/2)-C30	=D30/2	=I30-J30	29000000
27	36	0.5	24	0.5	61344	96	=F31*G31	=(B31/2)-C31	=D31/2	=I31-J31	29000000

Table 5. Continued.

t cap ring	t middle ring	t bottom ring	cap to ring dist	ring to ring dist	eff design angle
0.375	0	0.375	5	5	5.161886740
0.375	0	0.375	6	6	15.21055512
0.375	0	0.375	7	7	15.62767321
0.375	0.375	0.375	4	6	3.046799258
0.375	0.375	0.375	4	8	9.297616531
0.375	0.375	0.375	4	10	5.916883507
0.5	0	0.5	8	8	12.28461040
0.5	0	0.5	10	10	9.090861497
0.5	0	0.5	16	16	8.570748496
0.5	0.5	0.5	4	12	12.88641342
0.5	0.5	0.5	4	16	8.804457837
0.5	0.5	0.5	4	28	5.619724788
0.375	0	0.375	8	8	14.24432447
0.5	0	0.5	8	8	12.28461040
0.75	0	0.75	8	8	9.966144890
=M17	=M20	=O17	4	28	6.883986104
=M18	=M21	=O18	4	28	5.619724788
=M19	=M22	=O19	4	28	4.893962110
0.375	0	0.375	14	14	21.45234548
0.5	0	0.5	14	14	19.49263141
0.75	0	0.75	14	14	17.17416590
0.75	0	0.75	24	24	4.014071744
1	0	1	24	24	3.830223083
1.5	0	1.5	38	38	3.636503403
1	0	1	16	16	13.49856507
1	0	1	18	18	15.45658186
1	0	1	20	20	13.56851953

Table 5. Continued.

a	b	h
=J5*COS(RADIANS(R5))	=2*J5*SIN(RADIANS(R5))	=SQRT(S5^2-J5^2+I5^2)-S5
=J6*COS(RADIANS(R6))	=2*J6*SIN(RADIANS(R6))	=SQRT(S6^2-J6^2+I6^2)-S6
=J7*COS(RADIANS(R7))	=2*J7*SIN(RADIANS(R7))	=SQRT(S7^2-J7^2+I7^2)-S7
=J8*COS(RADIANS(R8))	=2*J8*SIN(RADIANS(R8))	=SQRT(S8^2-J8^2+I8^2)-S8
=J9*COS(RADIANS(R9))	=2*J9*SIN(RADIANS(R9))	=SQRT(S9^2-J9^2+I9^2)-S9
=J10*COS(RADIANS(R10))	=2*J10*SIN(RADIANS(R10))	=SQRT(S10^2-J10^2+I10^2)-S1(
=J11*COS(RADIANS(R11))	=2*J11*SIN(RADIANS(R11))	=SQRT(S11^2-J11^2+I11^2)-S11
=J12*COS(RADIANS(R12))	=2*J12*SIN(RADIANS(R12))	=SQRT(S12^2-J12^2+I12^2)-S12
=J13*COS(RADIANS(R13))	=2*J13*SIN(RADIANS(R13))	=SQRT(S13^2-J13^2+I13^2)-S13
=J14*COS(RADIANS(R14))	=2*J14*SIN(RADIANS(R14))	=SQRT(S14^2-J14^2+I14^2)-S14
=J15*COS(RADIANS(R15))	=2*J15*SIN(RADIANS(R15))	=SQRT(S15^2-J15^2+I15^2)-S15
=J16*COS(RADIANS(R16))	=2*J16*SIN(RADIANS(R16))	=SQRT(S16^2-J16^2+I16^2)-S16
=J17*COS(RADIANS(R17))	=2*J17*SIN(RADIANS(R17))	=SQRT(S17^2-J17^2+I17^2)-S17
=J18*COS(RADIANS(R18))	=2*J18*SIN(RADIANS(R18))	=SQRT(S18^2-J18^2+I18^2)-S18
=J19*COS(RADIANS(R19))	=2*J19*SIN(RADIANS(R19))	=SQRT(S19^2-J19^2+I19^2)-S19
=J20*COS(RADIANS(R20))	=2*J20*SIN(RADIANS(R20))	=SQRT(S20^2-J20^2+I20^2)-S2(
=J21*COS(RADIANS(R21))	=2*J21*SIN(RADIANS(R21))	=SQRT(S21^2-J21^2+I21^2)-S21
=J22*COS(RADIANS(R22))	=2*J22*SIN(RADIANS(R22))	=SQRT(S22^2-J22^2+I22^2)-S22
=J23*COS(RADIANS(R23))	=2*J23*SIN(RADIANS(R23))	=SQRT(S23^2-J23^2+I23^2)-S23
=J24*COS(RADIANS(R24))	=2*J24*SIN(RADIANS(R24))	=SQRT(S24^2-J24^2+I24^2)-S24
=J25*COS(RADIANS(R25))	=2*J25*SIN(RADIANS(R25))	=SQRT(S25^2-J25^2+I25^2)-S25
=J26*COS(RADIANS(R26))	=2*J26*SIN(RADIANS(R26))	=SQRT(S26^2-J26^2+I26^2)-S26
=J27*COS(RADIANS(R27))	=2*J27*SIN(RADIANS(R27))	=SQRT(S27^2-J27^2+I27^2)-S27
=J28*COS(RADIANS(R28))	=2*J28*SIN(RADIANS(R28))	=SQRT(S28^2-J28^2+I28^2)-S28
=J29*COS(RADIANS(R29))	=2*J29*SIN(RADIANS(R29))	=SQRT(S29^2-J29^2+I29^2)-S29
=J30*COS(RADIANS(R30))	=2*J30*SIN(RADIANS(R30))	=SQRT(S30^2-J30^2+I30^2)-S3(
=J31*COS(RADIANS(R31))	=2*J31*SIN(RADIANS(R31))	=SQRT(S31^2-J31^2+I31^2)-S31

Table 5. Continued.

column area cap	column area mid	column area bot	cap inertia s	middle ring inertia s	bottom ring inertia s
=M5*$T5	=N5*$T5	=O5*$T5	=(T5)^3*M5/12	=((T5)^3)*N5/12	=(T5^3)*O5/12
=M6*$T6	=N6*$T6	=O6*$T6	=(T6)^3*M6/12	=((T6)^3)*N6/12	=(T6^3)*O6/12
=M7*$T7	=N7*$T7	=O7*$T7	=(T7)^3*M7/12	=((T7)^3)*N7/12	=(T7^3)*O7/12
=M8*$T8	=N8*$T8	=O8*$T8	=(T8)^3*M8/12	=((T8)^3)*N8/12	=(T8^3)*O8/12
=M9*$T9	=N9*$T9	=O9*$T9	=(T9)^3*M9/12	=((T9)^3)*N9/12	=(T9^3)*O9/12
=M10*$T10	=N10*$T10	=O10*$T10	=(T10)^3*M10/12	=((T10)^3)*N10/12	=(T10^3)*O10/12
=M11*$T11	=N11*$T11	=O11*$T11	=(T11)^3*M11/12	=((T11)^3)*N11/12	=(T11^3)*O11/12
=M12*$T12	=N12*$T12	=O12*$T12	=(T12)^3*M12/12	=((T12)^3)*N12/12	=(T12^3)*O12/12
=M13*$T13	=N13*$T13	=O13*$T13	=(T13)^3*M13/12	=((T13)^3)*N13/12	=(T13^3)*O13/12
=M14*$T14	=N14*$T14	=O14*$T14	=(T14)^3*M14/12	=((T14)^3)*N14/12	=(T14^3)*O14/12
=M15*$T15	=N15*$T15	=O15*$T15	=(T15)^3*M15/12	=((T15)^3)*N15/12	=(T15^3)*O15/12
=M16*$T16	=N16*$T16	=O16*$T16	=(T16)^3*M16/12	=((T16)^3)*N16/12	=(T16^3)*O16/12
=M17*$T17	=N17*$T17	=O17*$T17	=(T17)^3*M17/12	=((T17)^3)*N17/12	=(T17^3)*O17/12
=M18*$T18	=N18*$T18	=O18*$T18	=(T18)^3*M18/12	=((T18)^3)*N18/12	=(T18^3)*O18/12
=M19*$T19	=N19*$T19	=O19*$T19	=(T19)^3*M19/12	=((T19)^3)*N19/12	=(T19^3)*O19/12
=M20*$T20	=N20*$T20	=O20*$T20	=(T20)^3*M20/12	=((T20)^3)*N20/12	=(T20^3)*O20/12
=M21*$T21	=N21*$T21	=O21*$T21	=(T21)^3*M21/12	=((T21)^3)*N21/12	=(T21^3)*O21/12
=M22*$T22	=N22*$T22	=O22*$T22	=(T22)^3*M22/12	=((T22)^3)*N22/12	=(T22^3)*O22/12
=M23*$T23	=N23*$T23	=O23*$T23	=(T23)^3*M23/12	=((T23)^3)*N23/12	=(T23^3)*O23/12
=M24*$T24	=N24*$T24	=O24*$T24	=(T24)^3*M24/12	=((T24)^3)*N24/12	=(T24^3)*O24/12
=M25*$T25	=N25*$T25	=O25*$T25	=(T25)^3*M25/12	=((T25)^3)*N25/12	=(T25^3)*O25/12
=M26*$T26	=N26*$T26	=O26*$T26	=(T26)^3*M26/12	=((T26)^3)*N26/12	=(T26^3)*O26/12
=M27*$T27	=N27*$T27	=O27*$T27	=(T27)^3*M27/12	=((T27)^3)*N27/12	=(T27^3)*O27/12
=M28*$T28	=N28*$T28	=O28*$T28	=(T28)^3*M28/12	=((T28)^3)*N28/12	=(T28^3)*O28/12
=M29*$T29	=N29*$T29	=O29*$T29	=(T29)^3*M29/12	=((T29)^3)*N29/12	=(T29^3)*O29/12
=M30*$T30	=N30*$T30	=O30*$T30	=(T30)^3*M30/12	=((T30)^3)*N30/12	=(T30^3)*O30/12
=M31*$T31	=N31*$T31	=O31*$T31	=(T31)^3*M31/12	=((T31)^3)*N31/12	=(T31^3)*O31/12

Table 5. Continued.

Cap top bending I	Mid top bending I	bot top bending I
=(M5^3)*$T5/12	=(N5^3)*$T5/12	=(O5^3)*$T5/12
=(M6^3)*$T6/12	=(N6^3)*$T6/12	=(O6^3)*$T6/12
=(M7^3)*$T7/12	=(N7^3)*$T7/12	=(O7^3)*$T7/12
=(M8^3)*$T8/12	=(N8^3)*$T8/12	=(O8^3)*$T8/12
=(M9^3)*$T9/12	=(N9^3)*$T9/12	=(O9^3)*$T9/12
=(M10^3)*$T10/12	=(N10^3)*$T10/12	=(O10^3)*$T10/12
=(M11^3)*$T11/12	=(N11^3)*$T11/12	=(O11^3)*$T11/12
=(M12^3)*$T12/12	=(N12^3)*$T12/12	=(O12^3)*$T12/12
=(M13^3)*$T13/12	=(N13^3)*$T13/12	=(O13^3)*$T13/12
=(M14^3)*$T14/12	=(N14^3)*$T14/12	=(O14^3)*$T14/12
=(M15^3)*$T15/12	=(N15^3)*$T15/12	=(O15^3)*$T15/12
=(M16^3)*$T16/12	=(N16^3)*$T16/12	=(O16^3)*$T16/12
=(M17^3)*$T17/12	=(N17^3)*$T17/12	=(O17^3)*$T17/12
=(M18^3)*$T18/12	=(N18^3)*$T18/12	=(O18^3)*$T18/12
=(M19^3)*$T19/12	=(N19^3)*$T19/12	=(O19^3)*$T19/12
=(M20^3)*$T20/12	=(N20^3)*$T20/12	=(O20^3)*$T20/12
=(M21^3)*$T21/12	=(N21^3)*$T21/12	=(O21^3)*$T21/12
=(M22^3)*$T22/12	=(N22^3)*$T22/12	=(O22^3)*$T22/12
=(M23^3)*$T23/12	=(N23^3)*$T23/12	=(O23^3)*$T23/12
=(M24^3)*$T24/12	=(N24^3)*$T24/12	=(O24^3)*$T24/12
=(M25^3)*$T25/12	=(N25^3)*$T25/12	=(O25^3)*$T25/12
=(M26^3)*$T26/12	=(N26^3)*$T26/12	=(O26^3)*$T26/12
=(M27^3)*$T27/12	=(N27^3)*$T27/12	=(O27^3)*$T27/12
=(M28^3)*$T28/12	=(N28^3)*$T28/12	=(O28^3)*$T28/12
=(M29^3)*$T29/12	=(N29^3)*$T29/12	=(O29^3)*$T29/12
=(M30^3)*$T30/12	=(N30^3)*$T30/12	=(O30^3)*$T30/12
=(M31^3)*$T31/12	=(N31^3)*$T31/12	=(O31^3)*$T31/12

Table 5. Continued.

cap stiffness	mid ring stiffness	bottom ring stiffness
=2*$L5*((W5/$U5)+(3*Z5/($U5^3)))	=2*$L5*((X5/$U5)+(3*AA5/($U5^3)))	=2*$L5*((Y5/$U5)+(3*AB5/($U5^3)))
=2*$L6*((W6/$U6)+(3*Z6/($U6^3)))	=2*$L6*((X6/$U6)+(3*AA6/($U6^3)))	=2*$L6*((Y6/$U6)+(3*AB6/($U6^3)))
=2*$L7*((W7/$U7)+(3*Z7/($U7^3)))	=2*$L7*((X7/$U7)+(3*AA7/($U7^3)))	=2*$L7*((Y7/$U7)+(3*AB7/($U7^3)))
=2*$L8*((W8/$U8)+(3*Z8/($U8^3)))	=2*$L8*((X8/$U8)+(3*AA8/($U8^3)))	=2*$L8*((Y8/$U8)+(3*AB8/($U8^3)))
=2*$L9*((W9/$U9)+(3*Z9/($U9^3)))	=2*$L9*((X9/$U9)+(3*AA9/($U9^3)))	=2*$L9*((Y9/$U9)+(3*AB9/($U9^3)))
=2*$L10*((W10/$U10)+(3*Z10/($U10^3)))	=2*$L10*((X10/$U10)+(3*AA10/($U10^3)))	=2*$L10*((Y10/$U10)+(3*AB10/($U10^3)))
=2*$L11*((W11/$U11)+(3*Z11/($U11^3)))	=2*$L11*((X11/$U11)+(3*AA11/($U11^3)))	=2*$L11*((Y11/$U11)+(3*AB11/($U11^3)))
=2*$L12*((W12/$U12)+(3*Z12/($U12^3)))	=2*$L12*((X12/$U12)+(3*AA12/($U12^3)))	=2*$L12*((Y12/$U12)+(3*AB12/($U12^3)))
=2*$L13*((W13/$U13)+(3*Z13/($U13^3)))	=2*$L13*((X13/$U13)+(3*AA13/($U13^3)))	=2*$L13*((Y13/$U13)+(3*AB13/($U13^3)))
=2*$L14*((W14/$U14)+(3*Z14/($U14^3)))	=2*$L14*((X14/$U14)+(3*AA14/($U14^3)))	=2*$L14*((Y14/$U14)+(3*AB14/($U14^3)))
=2*$L15*((W15/$U15)+(3*Z15/($U15^3)))	=2*$L15*((X15/$U15)+(3*AA15/($U15^3)))	=2*$L15*((Y15/$U15)+(3*AB15/($U15^3)))
=2*$L16*((W16/$U16)+(3*Z16/($U16^3)))	=2*$L16*((X16/$U16)+(3*AA16/($U16^3)))	=2*$L16*((Y16/$U16)+(3*AB16/($U16^3)))
=2*$L17*((W17/$U17)+(3*Z17/($U17^3)))	=2*$L17*((X17/$U17)+(3*AA17/($U17^3)))	=2*$L17*((Y17/$U17)+(3*AB17/($U17^3)))
=2*$L18*((W18/$U18)+(3*Z18/($U18^3)))	=2*$L18*((X18/$U18)+(3*AA18/($U18^3)))	=2*$L18*((Y18/$U18)+(3*AB18/($U18^3)))
=2*$L19*((W19/$U19)+(3*Z19/($U19^3)))	=2*$L19*((X19/$U19)+(3*AA19/($U19^3)))	=2*$L19*((Y19/$U19)+(3*AB19/($U19^3)))
=2*$L20*((W20/$U20)+(3*Z20/($U20^3)))	=2*$L20*((X20/$U20)+(3*AA20/($U20^3)))	=2*$L20*((Y20/$U20)+(3*AB20/($U20^3)))
=2*$L21*((W21/$U21)+(3*Z21/($U21^3)))	=2*$L21*((X21/$U21)+(3*AA21/($U21^3)))	=2*$L21*((Y21/$U21)+(3*AB21/($U21^3)))
=2*$L22*((W22/$U22)+(3*Z22/($U22^3)))	=2*$L22*((X22/$U22)+(3*AA22/($U22^3)))	=2*$L22*((Y22/$U22)+(3*AB22/($U22^3)))
=2*$L23*((W23/$U23)+(3*Z23/($U23^3)))	=2*$L23*((X23/$U23)+(3*AA23/($U23^3)))	=2*$L23*((Y23/$U23)+(3*AB23/($U23^3)))
=2*$L24*((W24/$U24)+(3*Z24/($U24^3)))	=2*$L24*((X24/$U24)+(3*AA24/($U24^3)))	=2*$L24*((Y24/$U24)+(3*AB24/($U24^3)))
=2*$L25*((W25/$U25)+(3*Z25/($U25^3)))	=2*$L25*((X25/$U25)+(3*AA25/($U25^3)))	=2*$L25*((Y25/$U25)+(3*AB25/($U25^3)))
=2*$L26*((W26/$U26)+(3*Z26/($U26^3)))	=2*$L26*((X26/$U26)+(3*AA26/($U26^3)))	=2*$L26*((Y26/$U26)+(3*AB26/($U26^3)))
=2*$L27*((W27/$U27)+(3*Z27/($U27^3)))	=2*$L27*((X27/$U27)+(3*AA27/($U27^3)))	=2*$L27*((Y27/$U27)+(3*AB27/($U27^3)))
=2*$L28*((W28/$U28)+(3*Z28/($U28^3)))	=2*$L28*((X28/$U28)+(3*AA28/($U28^3)))	=2*$L28*((Y28/$U28)+(3*AB28/($U28^3)))
=2*$L29*((W29/$U29)+(3*Z29/($U29^3)))	=2*$L29*((X29/$U29)+(3*AA29/($U29^3)))	=2*$L29*((Y29/$U29)+(3*AB29/($U29^3)))
=2*$L30*((W30/$U30)+(3*Z30/($U30^3)))	=2*$L30*((X30/$U30)+(3*AA30/($U30^3)))	=2*$L30*((Y30/$U30)+(3*AB30/($U30^3)))
=2*$L31*((W31/$U31)+(3*Z31/($U31^3)))	=2*$L31*((X31/$U31)+(3*AA31/($U31^3)))	=2*$L31*((Y31/$U31)+(3*AB31/($U31^3)))

Table 5. Continued.

cap stiffness bending	mid ring stiffness bending	bottom ring stiffness bending
=3*AC5*L5/$U5^3	=3*AD5*L5/$U5^3	=3*AE5*L5/$U5^3
=3*AC6*L6/$U6^3	=3*AD6*L6/$U6^3	=3*AE6*L6/$U6^3
=3*AC7*L7/$U7^3	=3*AD7*L7/$U7^3	=3*AE7*L7/$U7^3
=3*AC8*L8/$U8^3	=3*AD8*L8/$U8^3	=3*AE8*L8/$U8^3
=3*AC9*L9/$U9^3	=3*AD9*L9/$U9^3	=3*AE9*L9/$U9^3
=3*AC10*L10/$U10^3	=3*AD10*L10/$U10^3	=3*AE10*L10/$U10^3
=3*AC11*L11/$U11^3	=3*AD11*L11/$U11^3	=3*AE11*L11/$U11^3
=3*AC12*L12/$U12^3	=3*AD12*L12/$U12^3	=3*AE12*L12/$U12^3
=3*AC13*L13/$U13^3	=3*AD13*L13/$U13^3	=3*AE13*L13/$U13^3
=3*AC14*L14/$U14^3	=3*AD14*L14/$U14^3	=3*AE14*L14/$U14^3
=3*AC15*L15/$U15^3	=3*AD15*L15/$U15^3	=3*AE15*L15/$U15^3
=3*AC16*L16/$U16^3	=3*AD16*L16/$U16^3	=3*AE16*L16/$U16^3
=3*AC17*L17/$U17^3	=3*AD17*L17/$U17^3	=3*AE17*L17/$U17^3
=3*AC18*L18/$U18^3	=3*AD18*L18/$U18^3	=3*AE18*L18/$U18^3
=3*AC19*L19/$U19^3	=3*AD19*L19/$U19^3	=3*AE19*L19/$U19^3
=3*AC20*L20/$U20^3	=3*AD20*L20/$U20^3	=3*AE20*L20/$U20^3
=3*AC21*L21/$U21^3	=3*AD21*L21/$U21^3	=3*AE21*L21/$U21^3
=3*AC22*L22/$U22^3	=3*AD22*L22/$U22^3	=3*AE22*L22/$U22^3
=3*AC23*L23/$U23^3	=3*AD23*L23/$U23^3	=3*AE23*L23/$U23^3
=3*AC24*L24/$U24^3	=3*AD24*L24/$U24^3	=3*AE24*L24/$U24^3
=3*AC25*L25/$U25^3	=3*AD25*L25/$U25^3	=3*AE25*L25/$U25^3
=3*AC26*L26/$U26^3	=3*AD26*L26/$U26^3	=3*AE26*L26/$U26^3
=3*AC27*L27/$U27^3	=3*AD27*L27/$U27^3	=3*AE27*L27/$U27^3
=3*AC28*L28/$U28^3	=3*AD28*L28/$U28^3	=3*AE28*L28/$U28^3
=3*AC29*L29/$U29^3	=3*AD29*L29/$U29^3	=3*AE29*L29/$U29^3
=3*AC30*L30/$U30^3	=3*AD30*L30/$U30^3	=3*AE30*L30/$U30^3
=3*AC31*L31/$U31^3	=3*AD31*L31/$U31^3	=3*AE31*L31/$U31^3

Table 5. Continued.

sum of kixi	sum of ki	center of stiffness
=(AI5*2)+(AH5*(2+Q5))+(AG5*(2+Q5+P5))	=SUM(AG5:AI5)	=AN5/AO5-2
=(AI6*2)+(AH6*(2+Q6))+(AG6*(2+Q6+P6))	=SUM(AG6:AI6)	=AN6/AO6-2
=(AI7*2)+(AH7*(2+Q7))+(AG7*(2+Q7+P7))	=SUM(AG7:AI7)	=AN7/AO7-2
=(AI8*2)+(AH8*(2+Q8))+(AG8*(2+Q8+P8))	=SUM(AG8:AI8)	=AN8/AO8-2
=(AI9*2)+(AH9*(2+Q9))+(AG9*(2+Q9+P9))	=SUM(AG9:AI9)	=AN9/AO9-2
=(AI10*2)+(AH10*(2+Q10))+(AG10*(2+Q10+P10))	=SUM(AG10:AI10)	=AN10/AO10-2
=(AI11*2)+(AH11*(2+Q11))+(AG11*(2+Q11+P11))	=SUM(AG11:AI11)	=AN11/AO11-2
=(AI12*2)+(AH12*(2+Q12))+(AG12*(2+Q12+P12))	=SUM(AG12:AI12)	=AN12/AO12-2
=(AI13*2)+(AH13*(2+Q13))+(AG13*(2+Q13+P13))	=SUM(AG13:AI13)	=AN13/AO13-2
=(AI14*2)+(AH14*(2+Q14))+(AG14*(2+Q14+P14))	=SUM(AG14:AI14)	=AN14/AO14-2
=(AI15*2)+(AH15*(2+Q15))+(AG15*(2+Q15+P15))	=SUM(AG15:AI15)	=AN15/AO15-2
=(AI16*2)+(AH16*(2+Q16))+(AG16*(2+Q16+P16))	=SUM(AG16:AI16)	=AN16/AO16-2
=(AI17*2)+(AH17*(2+Q17))+(AG17*(2+Q17+P17))	=SUM(AG17:AI17)	=AN17/AO17-2
=(AI18*2)+(AH18*(2+Q18))+(AG18*(2+Q18+P18))	=SUM(AG18:AI18)	=AN18/AO18-2
=(AI19*2)+(AH19*(2+Q19))+(AG19*(2+Q19+P19))	=SUM(AG19:AI19)	=AN19/AO19-2
=(AI20*2)+(AH20*(2+Q20))+(AG20*(2+Q20+P20))	=SUM(AG20:AI20)	=AN20/AO20-2
=(AI21*2)+(AH21*(2+Q21))+(AG21*(2+Q21+P21))	=SUM(AG21:AI21)	=AN21/AO21-2
=(AI22*2)+(AH22*(2+Q22))+(AG22*(2+Q22+P22))	=SUM(AG22:AI22)	=AN22/AO22-2
=(AI23*2)+(AH23*(2+Q23))+(AG23*(2+Q23+P23))	=SUM(AG23:AI23)	=AN23/AO23-2
=(AI24*2)+(AH24*(2+Q24))+(AG24*(2+Q24+P24))	=SUM(AG24:AI24)	=AN24/AO24-2
=(AI25*2)+(AH25*(2+Q25))+(AG25*(2+Q25+P25))	=SUM(AG25:AI25)	=AN25/AO25-2
=(AI26*2)+(AH26*(2+Q26))+(AG26*(2+Q26+P26))	=SUM(AG26:AI26)	=AN26/AO26-2
=(AI27*2)+(AH27*(2+Q27))+(AG27*(2+Q27+P27))	=SUM(AG27:AI27)	=AN27/AO27-2
=(AI28*2)+(AH28*(2+Q28))+(AG28*(2+Q28+P28))	=SUM(AG28:AI28)	=AN28/AO28-2
=(AI29*2)+(AH29*(2+Q29))+(AG29*(2+Q29+P29))	=SUM(AG29:AI29)	=AN29/AO29-2
=(AI30*2)+(AH30*(2+Q30))+(AG30*(2+Q30+P30))	=SUM(AG30:AI30)	=AN30/AO30-2
=(AI31*2)+(AH31*(2+Q31))+(AG31*(2+Q31+P31))	=SUM(AG31:AI31)	=AN31/AO31-2

Table 5. Continued.

Moment Arms			
dcf	dc1	dc2	dc3
=G5+P5	=AP5	=Q5-AP5	=AS5+P5
=G6+P6	=AP6	=Q6-AP6	=AS6+P6
=G7+P7	=AP7	=Q7-AP7	=AS7+P7
=G8+P8	=AP8	=Q8-AP8	=AS8+P8
=G9+P9	=AP9	=Q9-AP9	=AS9+P9
=G10+P10	=AP10	=Q10-AP10	=AS10+P10
=G11+P11	=AP11	=Q11-AP11	=AS11+P11
=G12+P12	=AP12	=Q12-AP12	=AS12+P12
=G13+P13	=AP13	=Q13-AP13	=AS13+P13
=G14+P14	=AP14	=Q14-AP14	=AS14+P14
=G15+P15	=AP15	=Q15-AP15	=AS15+P15
=G16+P16	=AP16	=Q16-AP16	=AS16+P16
=G17+P17	=AP17	=Q17-AP17	=AS17+P17
=G18+P18	=AP18	=Q18-AP18	=AS18+P18
=G19+P19	=AP19	=Q19-AP19	=AS19+P19
=G20+P20	=AP20	=Q20-AP20	=AS20+P20
=G21+P21	=AP21	=Q21-AP21	=AS21+P21
=G22+P22	=AP22	=Q22-AP22	=AS22+P22
=G23+P23	=AP23	=Q23-AP23	=AS23+P23
=G24+P24	=AP24	=Q24-AP24	=AS24+P24
=G25+P25	=AP25	=Q25-AP25	=AS25+P25
=G26+P26	=AP26	=Q26-AP26	=AS26+P26
=G27+P27	=AP27	=Q27-AP27	=AS27+P27
=G28+P28	=AP28	=Q28-AP28	=AS28+P28
=G29+P29	=AP29	=Q29-AP29	=AS29+P29
=G30+P30	=AP30	=Q30-AP30	=AS30+P30
=G31+P31	=AP31	=Q31-AP31	=AS31+P31

Table 5. Continued.

x2	x1	x3	Theta (rad)
=(F5*AS5*(AR5+AQ5))/((AR5*(AS5*AH5+AT5*AG5))+(AS5^2*AH5)+(AT5^2*AG5))	=BD5/AI5	=BC5/AG5	=ATAN(AW5/AT5)
=(F6*AS6*(AR6+AQ6))/((AR6*(AS6*AH6+AT6*AG6))+(AS6^2*AH6)+(AT6^2*AG6))	=BD6/AI6	=BC6/AG6	=ATAN(AW6/AT6)
=(F7*AS7*(AR7+AQ7))/((AR7*(AS7*AH7+AT7*AG7))+(AS7^2*AH7)+(AT7^2*AG7))	=BD7/AI7	=BC7/AG7	=ATAN(AW7/AT7)
=(F8*AS8*(AR8+AQ8))/((AR8*(AS8*AH8+AT8*AG8))+(AS8^2*AH8)+(AT8^2*AG8))	=BD8/AI8	=BC8/AG8	=ATAN(AW8/AT8)
=(F9*AS9*(AR9+AQ9))/((AR9*(AS9*AH9+AT9*AG9))+(AS9^2*AH9)+(AT9^2*AG9))	=BD9/AI9	=BC9/AG9	=ATAN(AW9/AT9)
=(F10*AS10*(AR10+AQ10))/((AR10*(AS10*AH10+AT10*AG10))+(AS10^2*AH10)+(AT10^2*AG10))	=BD10/AI10	=BC10/AG10	=ATAN(AW10/AT10)
=(F11*AS11*(AR11+AQ11))/((AR11*(AS11*AH11+AT11*AG11))+(AS11^2*AH11)+(AT11^2*AG11))	=BD11/AI11	=BC11/AG11	=ATAN(AW11/AT11)
=(F12*AS12*(AR12+AQ12))/((AR12*(AS12*AH12+AT12*AG12))+(AS12^2*AH12)+(AT12^2*AG12))	=BD12/AI12	=BC12/AG12	=ATAN(AW12/AT12)
=(F13*AS13*(AR13+AQ13))/((AR13*(AS13*AH13+AT13*AG13))+(AS13^2*AH13)+(AT13^2*AG13))	=BD13/AI13	=BC13/AG13	=ATAN(AW13/AT13)
=(F14*AS14*(AR14+AQ14))/((AR14*(AS14*AH14+AT14*AG14))+(AS14^2*AH14)+(AT14^2*AG14))	=BD14/AI14	=BC14/AG14	=ATAN(AW14/AT14)
=(F15*AS15*(AR15+AQ15))/((AR15*(AS15*AH15+AT15*AG15))+(AS15^2*AH15)+(AT15^2*AG15))	=BD15/AI15	=BC15/AG15	=ATAN(AW15/AT15)
=(F16*AS16*(AR16+AQ16))/((AR16*(AS16*AH16+AT16*AG16))+(AS16^2*AH16)+(AT16^2*AG16))	=BD16/AI16	=BC16/AG16	=ATAN(AW16/AT16)
=(F17*AS17*(AR17+AQ17))/((AR17*(AS17*AH17+AT17*AG17))+(AS17^2*AH17)+(AT17^2*AG17))	=BD17/AI17	=BC17/AG17	=ATAN(AW17/AT17)
=(F18*AS18*(AR18+AQ18))/((AR18*(AS18*AH18+AT18*AG18))+(AS18^2*AH18)+(AT18^2*AG18))	=BD18/AI18	=BC18/AG18	=ATAN(AW18/AT18)
=(F19*AS19*(AR19+AQ19))/((AR19*(AS19*AH19+AT19*AG19))+(AS19^2*AH19)+(AT19^2*AG19))	=BD19/AI19	=BC19/AG19	=ATAN(AW19/AT19)
=(F20*AS20*(AR20+AQ20))/((AR20*(AS20*AH20+AT20*AG20))+(AS20^2*AH20)+(AT20^2*AG20))	=BD20/AI20	=BC20/AG20	=ATAN(AW20/AT20)
=(F21*AS21*(AR21+AQ21))/((AR21*(AS21*AH21+AT21*AG21))+(AS21^2*AH21)+(AT21^2*AG21))	=BD21/AI21	=BC21/AG21	=ATAN(AW21/AT21)
=(F22*AS22*(AR22+AQ22))/((AR22*(AS22*AH22+AT22*AG22))+(AS22^2*AH22)+(AT22^2*AG22))	=BD22/AI22	=BC22/AG22	=ATAN(AW22/AT22)
=(F23*AS23*(AR23+AQ23))/((AR23*(AS23*AH23+AT23*AG23))+(AS23^2*AH23)+(AT23^2*AG23))	=BD23/AI23	=BC23/AG23	=ATAN(AW23/AT23)
=(F24*AS24*(AR24+AQ24))/((AR24*(AS24*AH24+AT24*AG24))+(AS24^2*AH24)+(AT24^2*AG24))	=BD24/AI24	=BC24/AG24	=ATAN(AW24/AT24)
=(F25*AS25*(AR25+AQ25))/((AR25*(AS25*AH25+AT25*AG25))+(AS25^2*AH25)+(AT25^2*AG25))	=BD25/AI25	=BC25/AG25	=ATAN(AW25/AT25)
=(F26*AS26*(AR26+AQ26))/((AR26*(AS26*AH26+AT26*AG26))+(AS26^2*AH26)+(AT26^2*AG26))	=BD26/AI26	=BC26/AG26	=ATAN(AW26/AT26)
=(F27*AS27*(AR27+AQ27))/((AR27*(AS27*AH27+AT27*AG27))+(AS27^2*AH27)+(AT27^2*AG27))	=BD27/AI27	=BC27/AG27	=ATAN(AW27/AT27)
=(F28*AS28*(AR28+AQ28))/((AR28*(AS28*AH28+AT28*AG28))+(AS28^2*AH28)+(AT28^2*AG28))	=BD28/AI28	=BC28/AG28	=ATAN(AW28/AT28)
=(F29*AS29*(AR29+AQ29))/((AR29*(AS29*AH29+AT29*AG29))+(AS29^2*AH29)+(AT29^2*AG29))	=BD29/AI29	=BC29/AG29	=ATAN(AW29/AT29)
=(F30*AS30*(AR30+AQ30))/((AR30*(AS30*AH30+AT30*AG30))+(AS30^2*AH30)+(AT30^2*AG30))	=BD30/AI30	=BC30/AG30	=ATAN(AW30/AT30)
=(F31*AS31*(AR31+AQ31))/((AR31*(AS31*AH31+AT31*AG31))+(AS31^2*AH31)+(AT31^2*AG31))	=BD31/AI31	=BC31/AG31	=ATAN(AW31/AT31)

Table 5. Continued.

z1	z2
=AR5-($J5/(SIN(ATAN($J5/AR5))))*COS($AX5+ATAN($J5/AR5))	=AS5-($J5/(SIN(ATAN($J5/AS5))))*COS($AX5+ATAN($J5/AS5))
=AR6-($J6/(SIN(ATAN($J6/AR6))))*COS($AX6+ATAN($J6/AR6))	=AS6-($J6/(SIN(ATAN($J6/AS6))))*COS($AX6+ATAN($J6/AS6))
=AR7-($J7/(SIN(ATAN($J7/AR7))))*COS($AX7+ATAN($J7/AR7))	=AS7-($J7/(SIN(ATAN($J7/AS7))))*COS($AX7+ATAN($J7/AS7))
=AR8-($J8/(SIN(ATAN($J8/AR8))))*COS($AX8+ATAN($J8/AR8))	=AS8-($J8/(SIN(ATAN($J8/AS8))))*COS($AX8+ATAN($J8/AS8))
=AR9-($J9/(SIN(ATAN($J9/AR9))))*COS($AX9+ATAN($J9/AR9))	=AS9-($J9/(SIN(ATAN($J9/AS9))))*COS($AX9+ATAN($J9/AS9))
=AR10-($J10/(SIN(ATAN($J10/AR10))))*COS($AX10+ATAN($J10/AR10))	=AS10-($J10/(SIN(ATAN($J10/AS10))))*COS($AX10+ATAN($J10/AS10))
=AR11-($J11/(SIN(ATAN($J11/AR11))))*COS($AX11+ATAN($J11/AR11))	=AS11-($J11/(SIN(ATAN($J11/AS11))))*COS($AX11+ATAN($J11/AS11))
=AR12-($J12/(SIN(ATAN($J12/AR12))))*COS($AX12+ATAN($J12/AR12))	=AS12-($J12/(SIN(ATAN($J12/AS12))))*COS($AX12+ATAN($J12/AS12))
=AR13-($J13/(SIN(ATAN($J13/AR13))))*COS($AX13+ATAN($J13/AR13))	=AS13-($J13/(SIN(ATAN($J13/AS13))))*COS($AX13+ATAN($J13/AS13))
=AR14-($J14/(SIN(ATAN($J14/AR14))))*COS($AX14+ATAN($J14/AR14))	=AS14-($J14/(SIN(ATAN($J14/AS14))))*COS($AX14+ATAN($J14/AS14))
=AR15-($J15/(SIN(ATAN($J15/AR15))))*COS($AX15+ATAN($J15/AR15))	=AS15-($J15/(SIN(ATAN($J15/AS15))))*COS($AX15+ATAN($J15/AS15))
=AR16-($J16/(SIN(ATAN($J16/AR16))))*COS($AX16+ATAN($J16/AR16))	=AS16-($J16/(SIN(ATAN($J16/AS16))))*COS($AX16+ATAN($J16/AS16))
=AR17-($J17/(SIN(ATAN($J17/AR17))))*COS($AX17+ATAN($J17/AR17))	=AS17-($J17/(SIN(ATAN($J17/AS17))))*COS($AX17+ATAN($J17/AS17))
=AR18-($J18/(SIN(ATAN($J18/AR18))))*COS($AX18+ATAN($J18/AR18))	=AS18-($J18/(SIN(ATAN($J18/AS18))))*COS($AX18+ATAN($J18/AS18))
=AR19-($J19/(SIN(ATAN($J19/AR19))))*COS($AX19+ATAN($J19/AR19))	=AS19-($J19/(SIN(ATAN($J19/AS19))))*COS($AX19+ATAN($J19/AS19))
=AR20-($J20/(SIN(ATAN($J20/AR20))))*COS($AX20+ATAN($J20/AR20))	=AS20-($J20/(SIN(ATAN($J20/AS20))))*COS($AX20+ATAN($J20/AS20))
=AR21-($J21/(SIN(ATAN($J21/AR21))))*COS($AX21+ATAN($J21/AR21))	=AS21-($J21/(SIN(ATAN($J21/AS21))))*COS($AX21+ATAN($J21/AS21))
=AR22-($J22/(SIN(ATAN($J22/AR22))))*COS($AX22+ATAN($J22/AR22))	=AS22-($J22/(SIN(ATAN($J22/AS22))))*COS($AX22+ATAN($J22/AS22))
=AR23-($J23/(SIN(ATAN($J23/AR23))))*COS($AX23+ATAN($J23/AR23))	=AS23-($J23/(SIN(ATAN($J23/AS23))))*COS($AX23+ATAN($J23/AS23))
=AR24-($J24/(SIN(ATAN($J24/AR24))))*COS($AX24+ATAN($J24/AR24))	=AS24-($J24/(SIN(ATAN($J24/AS24))))*COS($AX24+ATAN($J24/AS24))
=AR25-($J25/(SIN(ATAN($J25/AR25))))*COS($AX25+ATAN($J25/AR25))	=AS25-($J25/(SIN(ATAN($J25/AS25))))*COS($AX25+ATAN($J25/AS25))
=AR26-($J26/(SIN(ATAN($J26/AR26))))*COS($AX26+ATAN($J26/AR26))	=AS26-($J26/(SIN(ATAN($J26/AS26))))*COS($AX26+ATAN($J26/AS26))
=AR27-($J27/(SIN(ATAN($J27/AR27))))*COS($AX27+ATAN($J27/AR27))	=AS27-($J27/(SIN(ATAN($J27/AS27))))*COS($AX27+ATAN($J27/AS27))
=AR28-($J28/(SIN(ATAN($J28/AR28))))*COS($AX28+ATAN($J28/AR28))	=AS28-($J28/(SIN(ATAN($J28/AS28))))*COS($AX28+ATAN($J28/AS28))
=AR29-($J29/(SIN(ATAN($J29/AR29))))*COS($AX29+ATAN($J29/AR29))	=AS29-($J29/(SIN(ATAN($J29/AS29))))*COS($AX29+ATAN($J29/AS29))
=AR30-($J30/(SIN(ATAN($J30/AR30))))*COS($AX30+ATAN($J30/AR30))	=AS30-($J30/(SIN(ATAN($J30/AS30))))*COS($AX30+ATAN($J30/AS30))
=AR31-($J31/(SIN(ATAN($J31/AR31))))*COS($AX31+ATAN($J31/AR31))	=AS31-($J31/(SIN(ATAN($J31/AS31))))*COS($AX31+ATAN($J31/AS31))

Table 5. Continued.

z3
=AT5-($J5/(SIN(ATAN($J5/AT5))))*COS($AX5+ATAN($J5/AT5))
=AT6-($J6/(SIN(ATAN($J6/AT6))))*COS($AX6+ATAN($J6/AT6))
=AT7-($J7/(SIN(ATAN($J7/AT7))))*COS($AX7+ATAN($J7/AT7))
=AT8-($J8/(SIN(ATAN($J8/AT8))))*COS($AX8+ATAN($J8/AT8))
=AT9-($J9/(SIN(ATAN($J9/AT9))))*COS($AX9+ATAN($J9/AT9))
=AT10-($J10/(SIN(ATAN($J10/AT10))))*COS($AX10+ATAN($J10/AT10))
=AT11-($J11/(SIN(ATAN($J11/AT11))))*COS($AX11+ATAN($J11/AT11))
=AT12-($J12/(SIN(ATAN($J12/AT12))))*COS($AX12+ATAN($J12/AT12))
=AT13-($J13/(SIN(ATAN($J13/AT13))))*COS($AX13+ATAN($J13/AT13))
=AT14-($J14/(SIN(ATAN($J14/AT14))))*COS($AX14+ATAN($J14/AT14))
=AT15-($J15/(SIN(ATAN($J15/AT15))))*COS($AX15+ATAN($J15/AT15))
=AT16-($J16/(SIN(ATAN($J16/AT16))))*COS($AX16+ATAN($J16/AT16))
=AT17-($J17/(SIN(ATAN($J17/AT17))))*COS($AX17+ATAN($J17/AT17))
=AT18-($J18/(SIN(ATAN($J18/AT18))))*COS($AX18+ATAN($J18/AT18))
=AT19-($J19/(SIN(ATAN($J19/AT19))))*COS($AX19+ATAN($J19/AT19))
=AT20-($J20/(SIN(ATAN($J20/AT20))))*COS($AX20+ATAN($J20/AT20))
=AT21-($J21/(SIN(ATAN($J21/AT21))))*COS($AX21+ATAN($J21/AT21))
=AT22-($J22/(SIN(ATAN($J22/AT22))))*COS($AX22+ATAN($J22/AT22))
=AT23-($J23/(SIN(ATAN($J23/AT23))))*COS($AX23+ATAN($J23/AT23))
=AT24-($J24/(SIN(ATAN($J24/AT24))))*COS($AX24+ATAN($J24/AT24))
=AT25-($J25/(SIN(ATAN($J25/AT25))))*COS($AX25+ATAN($J25/AT25))
=AT26-($J26/(SIN(ATAN($J26/AT26))))*COS($AX26+ATAN($J26/AT26))
=AT27-($J27/(SIN(ATAN($J27/AT27))))*COS($AX27+ATAN($J27/AT27))
=AT28-($J28/(SIN(ATAN($J28/AT28))))*COS($AX28+ATAN($J28/AT28))
=AT29-($J29/(SIN(ATAN($J29/AT29))))*COS($AX29+ATAN($J29/AT29))
=AT30-($J30/(SIN(ATAN($J30/AT30))))*COS($AX30+ATAN($J30/AT30))
=AT31-($J31/(SIN(ATAN($J31/AT31))))*COS($AX31+ATAN($J31/AT31))

Table 5. Continued.

mid ring	cap	bot ring
F2	F3	F1
=AU5*AH5	=((F5*(AR5+AQ5))-((AR5+AS5)*BB5))/(AR5+AT5)	=BB5+BC5-F5
=AU6*AH6	=((F6*(AR6+AQ6))-((AR6+AS6)*BB6))/(AR6+AT6)	=BB6+BC6-F6
=AU7*AH7	=((F7*(AR7+AQ7))-((AR7+AS7)*BB7))/(AR7+AT7)	=BB7+BC7-F7
=AU8*AH8	=((F8*(AR8+AQ8))-((AR8+AS8)*BB8))/(AR8+AT8)	=BB8+BC8-F8
=AU9*AH9	=((F9*(AR9+AQ9))-((AR9+AS9)*BB9))/(AR9+AT9)	=BB9+BC9-F9
=AU10*AH10	=((F10*(AR10+AQ10))-((AR10+AS10)*BB10))/(AR10+AT10)	=BB10+BC10-F10
=AU11*AH11	=((F11*(AR11+AQ11))-((AR11+AS11)*BB11))/(AR11+AT11)	=BB11+BC11-F11
=AU12*AH12	=((F12*(AR12+AQ12))-((AR12+AS12)*BB12))/(AR12+AT12)	=BB12+BC12-F12
=AU13*AH13	=((F13*(AR13+AQ13))-((AR13+AS13)*BB13))/(AR13+AT13)	=BB13+BC13-F13
=AU14*AH14	=((F14*(AR14+AQ14))-((AR14+AS14)*BB14))/(AR14+AT14)	=BB14+BC14-F14
=AU15*AH15	=((F15*(AR15+AQ15))-((AR15+AS15)*BB15))/(AR15+AT15)	=BB15+BC15-F15
=AU16*AH16	=((F16*(AR16+AQ16))-((AR16+AS16)*BB16))/(AR16+AT16)	=BB16+BC16-F16
=AU17*AH17	=((F17*(AR17+AQ17))-((AR17+AS17)*BB17))/(AR17+AT17)	=BB17+BC17-F17
=AU18*AH18	=((F18*(AR18+AQ18))-((AR18+AS18)*BB18))/(AR18+AT18)	=BB18+BC18-F18
=AU19*AH19	=((F19*(AR19+AQ19))-((AR19+AS19)*BB19))/(AR19+AT19)	=BB19+BC19-F19
=AU20*AH20	=((F20*(AR20+AQ20))-((AR20+AS20)*BB20))/(AR20+AT20)	=BB20+BC20-F20
=AU21*AH21	=((F21*(AR21+AQ21))-((AR21+AS21)*BB21))/(AR21+AT21)	=BB21+BC21-F21
=AU22*AH22	=((F22*(AR22+AQ22))-((AR22+AS22)*BB22))/(AR22+AT22)	=BB22+BC22-F22
=AU23*AH23	=((F23*(AR23+AQ23))-((AR23+AS23)*BB23))/(AR23+AT23)	=BB23+BC23-F23
=AU24*AH24	=((F24*(AR24+AQ24))-((AR24+AS24)*BB24))/(AR24+AT24)	=BB24+BC24-F24
=AU25*AH25	=((F25*(AR25+AQ25))-((AR25+AS25)*BB25))/(AR25+AT25)	=BB25+BC25-F25
=AU26*AH26	=((F26*(AR26+AQ26))-((AR26+AS26)*BB26))/(AR26+AT26)	=BB26+BC26-F26
=AU27*AH27	=((F27*(AR27+AQ27))-((AR27+AS27)*BB27))/(AR27+AT27)	=BB27+BC27-F27
=AU28*AH28	=((F28*(AR28+AQ28))-((AR28+AS28)*BB28))/(AR28+AT28)	=BB28+BC28-F28
=AU29*AH29	=((F29*(AR29+AQ29))-((AR29+AS29)*BB29))/(AR29+AT29)	=BB29+BC29-F29
=AU30*AH30	=((F30*(AR30+AQ30))-((AR30+AS30)*BB30))/(AR30+AT30)	=BB30+BC30-F30
=AU31*AH31	=((F31*(AR31+AQ31))-((AR31+AS31)*BB31))/(AR31+AT31)	=BB31+BC31-F31

Table 5. Continued.

Column relative stiffness		
cap	mid ring	bot ring
=0.5*(W5/$U5)/((W5/$U5)+(3*Z5/($U5^3)))	=0.5*(X5/$U5)/((X5/$U5)+(3*AA5/($U5^3)))	=0.5*(Y5/$U5)/((Y5/$U5)+(3*AB5/($U5^3)))
=0.5*(W6/$U6)/((W6/$U6)+(3*Z6/($U6^3)))	=0.5*(X6/$U6)/((X6/$U6)+(3*AA6/($U6^3)))	=0.5*(Y6/$U6)/((Y6/$U6)+(3*AB6/($U6^3)))
=0.5*(W7/$U7)/((W7/$U7)+(3*Z7/($U7^3)))	=0.5*(X7/$U7)/((X7/$U7)+(3*AA7/($U7^3)))	=0.5*(Y7/$U7)/((Y7/$U7)+(3*AB7/($U7^3)))
=0.5*(W8/$U8)/((W8/$U8)+(3*Z8/($U8^3)))	=0.5*(X8/$U8)/((X8/$U8)+(3*AA8/($U8^3)))	=0.5*(Y8/$U8)/((Y8/$U8)+(3*AB8/($U8^3)))
=0.5*(W9/$U9)/((W9/$U9)+(3*Z9/($U9^3)))	=0.5*(X9/$U9)/((X9/$U9)+(3*AA9/($U9^3)))	=0.5*(Y9/$U9)/((Y9/$U9)+(3*AB9/($U9^3)))
=0.5*(W10/$U10)/((W10/$U10)+(3*Z10/($U10^3)))	=0.5*(X10/$U10)/((X10/$U10)+(3*AA10/($U10^3)))	=0.5*(Y10/$U10)/((Y10/$U10)+(3*AB10/($U10^3)))
=0.5*(W11/$U11)/((W11/$U11)+(3*Z11/($U11^3)))	=0.5*(X11/$U11)/((X11/$U11)+(3*AA11/($U11^3)))	=0.5*(Y11/$U11)/((Y11/$U11)+(3*AB11/($U11^3)))
=0.5*(W12/$U12)/((W12/$U12)+(3*Z12/($U12^3)))	=0.5*(X12/$U12)/((X12/$U12)+(3*AA12/($U12^3)))	=0.5*(Y12/$U12)/((Y12/$U12)+(3*AB12/($U12^3)))
=0.5*(W13/$U13)/((W13/$U13)+(3*Z13/($U13^3)))	=0.5*(X13/$U13)/((X13/$U13)+(3*AA13/($U13^3)))	=0.5*(Y13/$U13)/((Y13/$U13)+(3*AB13/($U13^3)))
=0.5*(W14/$U14)/((W14/$U14)+(3*Z14/($U14^3)))	=0.5*(X14/$U14)/((X14/$U14)+(3*AA14/($U14^3)))	=0.5*(Y14/$U14)/((Y14/$U14)+(3*AB14/($U14^3)))
=0.5*(W15/$U15)/((W15/$U15)+(3*Z15/($U15^3)))	=0.5*(X15/$U15)/((X15/$U15)+(3*AA15/($U15^3)))	=0.5*(Y15/$U15)/((Y15/$U15)+(3*AB15/($U15^3)))
=0.5*(W16/$U16)/((W16/$U16)+(3*Z16/($U16^3)))	=0.5*(X16/$U16)/((X16/$U16)+(3*AA16/($U16^3)))	=0.5*(Y16/$U16)/((Y16/$U16)+(3*AB16/($U16^3)))
=0.5*(W17/$U17)/((W17/$U17)+(3*Z17/($U17^3)))	=0.5*(X17/$U17)/((X17/$U17)+(3*AA17/($U17^3)))	=0.5*(Y17/$U17)/((Y17/$U17)+(3*AB17/($U17^3)))
=0.5*(W18/$U18)/((W18/$U18)+(3*Z18/($U18^3)))	=0.5*(X18/$U18)/((X18/$U18)+(3*AA18/($U18^3)))	=0.5*(Y18/$U18)/((Y18/$U18)+(3*AB18/($U18^3)))
=0.5*(W19/$U19)/((W19/$U19)+(3*Z19/($U19^3)))	=0.5*(X19/$U19)/((X19/$U19)+(3*AA19/($U19^3)))	=0.5*(Y19/$U19)/((Y19/$U19)+(3*AB19/($U19^3)))
=0.5*(W20/$U20)/((W20/$U20)+(3*Z20/($U20^3)))	=0.5*(X20/$U20)/((X20/$U20)+(3*AA20/($U20^3)))	=0.5*(Y20/$U20)/((Y20/$U20)+(3*AB20/($U20^3)))
=0.5*(W21/$U21)/((W21/$U21)+(3*Z21/($U21^3)))	=0.5*(X21/$U21)/((X21/$U21)+(3*AA21/($U21^3)))	=0.5*(Y21/$U21)/((Y21/$U21)+(3*AB21/($U21^3)))
=0.5*(W22/$U22)/((W22/$U22)+(3*Z22/($U22^3)))	=0.5*(X22/$U22)/((X22/$U22)+(3*AA22/($U22^3)))	=0.5*(Y22/$U22)/((Y22/$U22)+(3*AB22/($U22^3)))
=0.5*(W23/$U23)/((W23/$U23)+(3*Z23/($U23^3)))	=0.5*(X23/$U23)/((X23/$U23)+(3*AA23/($U23^3)))	=0.5*(Y23/$U23)/((Y23/$U23)+(3*AB23/($U23^3)))
=0.5*(W24/$U24)/((W24/$U24)+(3*Z24/($U24^3)))	=0.5*(X24/$U24)/((X24/$U24)+(3*AA24/($U24^3)))	=0.5*(Y24/$U24)/((Y24/$U24)+(3*AB24/($U24^3)))
=0.5*(W25/$U25)/((W25/$U25)+(3*Z25/($U25^3)))	=0.5*(X25/$U25)/((X25/$U25)+(3*AA25/($U25^3)))	=0.5*(Y25/$U25)/((Y25/$U25)+(3*AB25/($U25^3)))
=0.5*(W26/$U26)/((W26/$U26)+(3*Z26/($U26^3)))	=0.5*(X26/$U26)/((X26/$U26)+(3*AA26/($U26^3)))	=0.5*(Y26/$U26)/((Y26/$U26)+(3*AB26/($U26^3)))
=0.5*(W27/$U27)/((W27/$U27)+(3*Z27/($U27^3)))	=0.5*(X27/$U27)/((X27/$U27)+(3*AA27/($U27^3)))	=0.5*(Y27/$U27)/((Y27/$U27)+(3*AB27/($U27^3)))
=0.5*(W28/$U28)/((W28/$U28)+(3*Z28/($U28^3)))	=0.5*(X28/$U28)/((X28/$U28)+(3*AA28/($U28^3)))	=0.5*(Y28/$U28)/((Y28/$U28)+(3*AB28/($U28^3)))
=0.5*(W29/$U29)/((W29/$U29)+(3*Z29/($U29^3)))	=0.5*(X29/$U29)/((X29/$U29)+(3*AA29/($U29^3)))	=0.5*(Y29/$U29)/((Y29/$U29)+(3*AB29/($U29^3)))
=0.5*(W30/$U30)/((W30/$U30)+(3*Z30/($U30^3)))	=0.5*(X30/$U30)/((X30/$U30)+(3*AA30/($U30^3)))	=0.5*(Y30/$U30)/((Y30/$U30)+(3*AB30/($U30^3)))
=0.5*(W31/$U31)/((W31/$U31)+(3*Z31/($U31^3)))	=0.5*(X31/$U31)/((X31/$U31)+(3*AA31/($U31^3)))	=0.5*(Y31/$U31)/((Y31/$U31)+(3*AB31/($U31^3)))

Table 5. Continued.

Beam relative stiffness			Column stress		
cap	mid ring	bot ring	cap	mid ring	bot ring
=0.5-BE5	=0.5-BF5	=0.5-BG5	=BC5*BE5/W5	=BB5*BF5/X5	=BD5*BG5/Y5
=0.5-BE6	=0.5-BF6	=0.5-BG6	=BC6*BE6/W6	=BB6*BF6/X6	=BD6*BG6/Y6
=0.5-BE7	=0.5-BF7	=0.5-BG7	=BC7*BE7/W7	=BB7*BF7/X7	=BD7*BG7/Y7
=0.5-BE8	=0.5-BF8	=0.5-BG8	=BC8*BE8/W8	=BB8*BF8/X8	=BD8*BG8/Y8
=0.5-BE9	=0.5-BF9	=0.5-BG9	=BC9*BE9/W9	=BB9*BF9/X9	=BD9*BG9/Y9
=0.5-BE10	=0.5-BF10	=0.5-BG10	=BC10*BE10/W10	=BB10*BF10/X10	=BD10*BG10/Y10
=0.5-BE11	=0.5-BF11	=0.5-BG11	=BC11*BE11/W11	=BB11*BF11/X11	=BD11*BG11/Y11
=0.5-BE12	=0.5-BF12	=0.5-BG12	=BC12*BE12/W12	=BB12*BF12/X12	=BD12*BG12/Y12
=0.5-BE13	=0.5-BF13	=0.5-BG13	=BC13*BE13/W13	=BB13*BF13/X13	=BD13*BG13/Y13
=0.5-BE14	=0.5-BF14	=0.5-BG14	=BC14*BE14/W14	=BB14*BF14/X14	=BD14*BG14/Y14
=0.5-BE15	=0.5-BF15	=0.5-BG15	=BC15*BE15/W15	=BB15*BF15/X15	=BD15*BG15/Y15
=0.5-BE16	=0.5-BF16	=0.5-BG16	=BC16*BE16/W16	=BB16*BF16/X16	=BD16*BG16/Y16
=0.5-BE17	=0.5-BF17	=0.5-BG17	=BC17*BE17/W17	=BB17*BF17/X17	=BD17*BG17/Y17
=0.5-BE18	=0.5-BF18	=0.5-BG18	=BC18*BE18/W18	=BB18*BF18/X18	=BD18*BG18/Y18
=0.5-BE19	=0.5-BF19	=0.5-BG19	=BC19*BE19/W19	=BB19*BF19/X19	=BD19*BG19/Y19
=0.5-BE20	=0.5-BF20	=0.5-BG20	=BC20*BE20/W20	=BB20*BF20/X20	=BD20*BG20/Y20
=0.5-BE21	=0.5-BF21	=0.5-BG21	=BC21*BE21/W21	=BB21*BF21/X21	=BD21*BG21/Y21
=0.5-BE22	=0.5-BF22	=0.5-BG22	=BC22*BE22/W22	=BB22*BF22/X22	=BD22*BG22/Y22
=0.5-BE23	=0.5-BF23	=0.5-BG23	=BC23*BE23/W23	=BB23*BF23/X23	=BD23*BG23/Y23
=0.5-BE24	=0.5-BF24	=0.5-BG24	=BC24*BE24/W24	=BB24*BF24/X24	=BD24*BG24/Y24
=0.5-BE25	=0.5-BF25	=0.5-BG25	=BC25*BE25/W25	=BB25*BF25/X25	=BD25*BG25/Y25
=0.5-BE26	=0.5-BF26	=0.5-BG26	=BC26*BE26/W26	=BB26*BF26/X26	=BD26*BG26/Y26
=0.5-BE27	=0.5-BF27	=0.5-BG27	=BC27*BE27/W27	=BB27*BF27/X27	=BD27*BG27/Y27
=0.5-BE28	=0.5-BF28	=0.5-BG28	=BC28*BE28/W28	=BB28*BF28/X28	=BD28*BG28/Y28
=0.5-BE29	=0.5-BF29	=0.5-BG29	=BC29*BE29/W29	=BB29*BF29/X29	=BD29*BG29/Y29
=0.5-BE30	=0.5-BF30	=0.5-BG30	=BC30*BE30/W30	=BB30*BF30/X30	=BD30*BG30/Y30
=0.5-BE31	=0.5-BF31	=0.5-BG31	=BC31*BE31/W31	=BB31*BF31/X31	=BD31*BG31/Y31

Table 5. Continued.

beam stress			mid ring	cap	bot ring
cap	mid ring	bot ring	Fz2 top	Fz3 top	Fz1 top
=BC5*$U5*($T5/2)*BH5/Z5	=BB5*$U5*($T5/2)*BI5/AA5	=BD5*$U5*($T5/2)*BJ5/AB5	=AZ5*AK5	=BA5*AJ5	=AY5*AL5
=BC6*$U6*($T6/2)*BH6/Z6	=BB6*$U6*($T6/2)*BI6/AA6	=BD6*$U6*($T6/2)*BJ6/AB6	=AZ6*AK6	=BA6*AJ6	=AY6*AL6
=BC7*$U7*($T7/2)*BH7/Z7	=BB7*$U7*($T7/2)*BI7/AA7	=BD7*$U7*($T7/2)*BJ7/AB7	=AZ7*AK7	=BA7*AJ7	=AY7*AL7
=BC8*$U8*($T8/2)*BH8/Z8	=BB8*$U8*($T8/2)*BI8/AA8	=BD8*$U8*($T8/2)*BJ8/AB8	=AZ8*AK8	=BA8*AJ8	=AY8*AL8
=BC9*$U9*($T9/2)*BH9/Z9	=BB9*$U9*($T9/2)*BI9/AA9	=BD9*$U9*($T9/2)*BJ9/AB9	=AZ9*AK9	=BA9*AJ9	=AY9*AL9
=BC10*$U10*($T10/2)*BH10/Z10	=BB10*$U10*($T10/2)*BI10/AA10	=BD10*$U10*($T10/2)*BJ10/AB10	=AZ10*AK10	=BA10*AJ10	=AY10*AL10
=BC11*$U11*($T11/2)*BH11/Z11	=BB11*$U11*($T11/2)*BI11/AA11	=BD11*$U11*($T11/2)*BJ11/AB11	=AZ11*AK11	=BA11*AJ11	=AY11*AL11
=BC12*$U12*($T12/2)*BH12/Z12	=BB12*$U12*($T12/2)*BI12/AA12	=BD12*$U12*($T12/2)*BJ12/AB12	=AZ12*AK12	=BA12*AJ12	=AY12*AL12
=BC13*$U13*($T13/2)*BH13/Z13	=BB13*$U13*($T13/2)*BI13/AA13	=BD13*$U13*($T13/2)*BJ13/AB13	=AZ13*AK13	=BA13*AJ13	=AY13*AL13
=BC14*$U14*($T14/2)*BH14/Z14	=BB14*$U14*($T14/2)*BI14/AA14	=BD14*$U14*($T14/2)*BJ14/AB14	=AZ14*AK14	=BA14*AJ14	=AY14*AL14
=BC15*$U15*($T15/2)*BH15/Z15	=BB15*$U15*($T15/2)*BI15/AA15	=BD15*$U15*($T15/2)*BJ15/AB15	=AZ15*AK15	=BA15*AJ15	=AY15*AL15
=BC16*$U16*($T16/2)*BH16/Z16	=BB16*$U16*($T16/2)*BI16/AA16	=BD16*$U16*($T16/2)*BJ16/AB16	=AZ16*AK16	=BA16*AJ16	=AY16*AL16
=BC17*$U17*($T17/2)*BH17/Z17	=BB17*$U17*($T17/2)*BI17/AA17	=BD17*$U17*($T17/2)*BJ17/AB17	=AZ17*AK17	=BA17*AJ17	=AY17*AL17
=BC18*$U18*($T18/2)*BH18/Z18	=BB18*$U18*($T18/2)*BI18/AA18	=BD18*$U18*($T18/2)*BJ18/AB18	=AZ18*AK18	=BA18*AJ18	=AY18*AL18
=BC19*$U19*($T19/2)*BH19/Z19	=BB19*$U19*($T19/2)*BI19/AA19	=BD19*$U19*($T19/2)*BJ19/AB19	=AZ19*AK19	=BA19*AJ19	=AY19*AL19
=BC20*$U20*($T20/2)*BH20/Z20	=BB20*$U20*($T20/2)*BI20/AA20	=BD20*$U20*($T20/2)*BJ20/AB20	=AZ20*AK20	=BA20*AJ20	=AY20*AL20
=BC21*$U21*($T21/2)*BH21/Z21	=BB21*$U21*($T21/2)*BI21/AA21	=BD21*$U21*($T21/2)*BJ21/AB21	=AZ21*AK21	=BA21*AJ21	=AY21*AL21
=BC22*$U22*($T22/2)*BH22/Z22	=BB22*$U22*($T22/2)*BI22/AA22	=BD22*$U22*($T22/2)*BJ22/AB22	=AZ22*AK22	=BA22*AJ22	=AY22*AL22
=BC23*$U23*($T23/2)*BH23/Z23	=BB23*$U23*($T23/2)*BI23/AA23	=BD23*$U23*($T23/2)*BJ23/AB23	=AZ23*AK23	=BA23*AJ23	=AY23*AL23
=BC24*$U24*($T24/2)*BH24/Z24	=BB24*$U24*($T24/2)*BI24/AA24	=BD24*$U24*($T24/2)*BJ24/AB24	=AZ24*AK24	=BA24*AJ24	=AY24*AL24
=BC25*$U25*($T25/2)*BH25/Z25	=BB25*$U25*($T25/2)*BI25/AA25	=BD25*$U25*($T25/2)*BJ25/AB25	=AZ25*AK25	=BA25*AJ25	=AY25*AL25
=BC26*$U26*($T26/2)*BH26/Z26	=BB26*$U26*($T26/2)*BI26/AA26	=BD26*$U26*($T26/2)*BJ26/AB26	=AZ26*AK26	=BA26*AJ26	=AY26*AL26
=BC27*$U27*($T27/2)*BH27/Z27	=BB27*$U27*($T27/2)*BI27/AA27	=BD27*$U27*($T27/2)*BJ27/AB27	=AZ27*AK27	=BA27*AJ27	=AY27*AL27
=BC28*$U28*($T28/2)*BH28/Z28	=BB28*$U28*($T28/2)*BI28/AA28	=BD28*$U28*($T28/2)*BJ28/AB28	=AZ28*AK28	=BA28*AJ28	=AY28*AL28
=BC29*$U29*($T29/2)*BH29/Z29	=BB29*$U29*($T29/2)*BI29/AA29	=BD29*$U29*($T29/2)*BJ29/AB29	=AZ29*AK29	=BA29*AJ29	=AY29*AL29
=BC30*$U30*($T30/2)*BH30/Z30	=BB30*$U30*($T30/2)*BI30/AA30	=BD30*$U30*($T30/2)*BJ30/AB30	=AZ30*AK30	=BA30*AJ30	=AY30*AL30
=BC31*$U31*($T31/2)*BH31/Z31	=BB31*$U31*($T31/2)*BI31/AA31	=BD31*$U31*($T31/2)*BJ31/AB31	=AZ31*AK31	=BA31*AJ31	=AY31*AL31

Table 5. Continued.

bending stress		
cap	mid ring	bot ring
=BR5*$U5*(M5/2)/AC5	=BQ5*U5*(N5/2)/AD5	=BS5*U5*(O5/2)/AE5
=BR6*$U6*(M6/2)/AC6	=BQ6*U6*(N6/2)/AD6	=BS6*U6*(O6/2)/AE6
=BR7*$U7*(M7/2)/AC7	=BQ7*U7*(N7/2)/AD7	=BS7*U7*(O7/2)/AE7
=BR8*$U8*(M8/2)/AC8	=BQ8*U8*(N8/2)/AD8	=BS8*U8*(O8/2)/AE8
=BR9*$U9*(M9/2)/AC9	=BQ9*U9*(N9/2)/AD9	=BS9*U9*(O9/2)/AE9
=BR10*$U10*(M10/2)/AC1(	=BQ10*U10*(N10/2)/AD1(	=BS10*U10*(O10/2)/AE10
=BR11*$U11*(M11/2)/AC11	=BQ11*U11*(N11/2)/AD11	=BS11*U11*(O11/2)/AE11
=BR12*$U12*(M12/2)/AC12	=BQ12*U12*(N12/2)/AD12	=BS12*U12*(O12/2)/AE12
=BR13*$U13*(M13/2)/AC13	=BQ13*U13*(N13/2)/AD13	=BS13*U13*(O13/2)/AE13
=BR14*$U14*(M14/2)/AC14	=BQ14*U14*(N14/2)/AD14	=BS14*U14*(O14/2)/AE14
=BR15*$U15*(M15/2)/AC15	=BQ15*U15*(N15/2)/AD15	=BS15*U15*(O15/2)/AE15
=BR16*$U16*(M16/2)/AC16	=BQ16*U16*(N16/2)/AD16	=BS16*U16*(O16/2)/AE16
=BR17*$U17*(M17/2)/AC17	=BQ17*U17*(N17/2)/AD17	=BS17*U17*(O17/2)/AE17
=BR18*$U18*(M18/2)/AC18	=BQ18*U18*(N18/2)/AD18	=BS18*U18*(O18/2)/AE18
=BR19*$U19*(M19/2)/AC19	=BQ19*U19*(N19/2)/AD19	=BS19*U19*(O19/2)/AE19
=BR20*$U20*(M20/2)/AC2(	=BQ20*U20*(N20/2)/AD2(	=BS20*U20*(O20/2)/AE20
=BR21*$U21*(M21/2)/AC21	=BQ21*U21*(N21/2)/AD21	=BS21*U21*(O21/2)/AE21
=BR22*$U22*(M22/2)/AC22	=BQ22*U22*(N22/2)/AD22	=BS22*U22*(O22/2)/AE22
=BR23*$U23*(M23/2)/AC23	=BQ23*U23*(N23/2)/AD23	=BS23*U23*(O23/2)/AE23
=BR24*$U24*(M24/2)/AC24	=BQ24*U24*(N24/2)/AD24	=BS24*U24*(O24/2)/AE24
=BR25*$U25*(M25/2)/AC25	=BQ25*U25*(N25/2)/AD25	=BS25*U25*(O25/2)/AE25
=BR26*$U26*(M26/2)/AC26	=BQ26*U26*(N26/2)/AD26	=BS26*U26*(O26/2)/AE26
=BR27*$U27*(M27/2)/AC27	=BQ27*U27*(N27/2)/AD27	=BS27*U27*(O27/2)/AE27
=BR28*$U28*(M28/2)/AC28	=BQ28*U28*(N28/2)/AD28	=BS28*U28*(O28/2)/AE28
=BR29*$U29*(M29/2)/AC29	=BQ29*U29*(N29/2)/AD29	=BS29*U29*(O29/2)/AE29
=BR30*$U30*(M30/2)/AC3(	=BQ30*U30*(N30/2)/AD3(	=BS30*U30*(O30/2)/AE30
=BR31*$U31*(M31/2)/AC31	=BQ31*U31*(N31/2)/AD31	=BS31*U31*(O31/2)/AE31

Table 5. Continued.

combined stress		
cap	mid ring	bot ring
=ABS(BT5)+ABS(BK5)	=ABS(BU5)+ABS(BL5)	=ABS(BV5)+ABS(BM5)
=ABS(BT6)+ABS(BK6)	=ABS(BU6)+ABS(BL6)	=ABS(BV6)+ABS(BM6)
=ABS(BT7)+ABS(BK7)	=ABS(BU7)+ABS(BL7)	=ABS(BV7)+ABS(BM7)
=ABS(BT8)+ABS(BK8)	=ABS(BU8)+ABS(BL8)	=ABS(BV8)+ABS(BM8)
=ABS(BT9)+ABS(BK9)	=ABS(BU9)+ABS(BL9)	=ABS(BV9)+ABS(BM9)
=ABS(BT10)+ABS(BK10)	=ABS(BU10)+ABS(BL10)	=ABS(BV10)+ABS(BM10)
=ABS(BT11)+ABS(BK11)	=ABS(BU11)+ABS(BL11)	=ABS(BV11)+ABS(BM11)
=ABS(BT12)+ABS(BK12)	=ABS(BU12)+ABS(BL12)	=ABS(BV12)+ABS(BM12)
=ABS(BT13)+ABS(BK13)	=ABS(BU13)+ABS(BL13)	=ABS(BV13)+ABS(BM13)
=ABS(BT14)+ABS(BK14)	=ABS(BU14)+ABS(BL14)	=ABS(BV14)+ABS(BM14)
=ABS(BT15)+ABS(BK15)	=ABS(BU15)+ABS(BL15)	=ABS(BV15)+ABS(BM15)
=ABS(BT16)+ABS(BK16)	=ABS(BU16)+ABS(BL16)	=ABS(BV16)+ABS(BM16)
=ABS(BT17)+ABS(BK17)	=ABS(BU17)+ABS(BL17)	=ABS(BV17)+ABS(BM17)
=ABS(BT18)+ABS(BK18)	=ABS(BU18)+ABS(BL18)	=ABS(BV18)+ABS(BM18)
=ABS(BT19)+ABS(BK19)	=ABS(BU19)+ABS(BL19)	=ABS(BV19)+ABS(BM19)
=ABS(BT20)+ABS(BK20)	=ABS(BU20)+ABS(BL20)	=ABS(BV20)+ABS(BM20)
=ABS(BT21)+ABS(BK21)	=ABS(BU21)+ABS(BL21)	=ABS(BV21)+ABS(BM21)
=ABS(BT22)+ABS(BK22)	=ABS(BU22)+ABS(BL22)	=ABS(BV22)+ABS(BM22)
=ABS(BT23)+ABS(BK23)	=ABS(BU23)+ABS(BL23)	=ABS(BV23)+ABS(BM23)
=ABS(BT24)+ABS(BK24)	=ABS(BU24)+ABS(BL24)	=ABS(BV24)+ABS(BM24)
=ABS(BT25)+ABS(BK25)	=ABS(BU25)+ABS(BL25)	=ABS(BV25)+ABS(BM25)
=ABS(BT26)+ABS(BK26)	=ABS(BU26)+ABS(BL26)	=ABS(BV26)+ABS(BM26)
=ABS(BT27)+ABS(BK27)	=ABS(BU27)+ABS(BL27)	=ABS(BV27)+ABS(BM27)
=ABS(BT28)+ABS(BK28)	=ABS(BU28)+ABS(BL28)	=ABS(BV28)+ABS(BM28)
=ABS(BT29)+ABS(BK29)	=ABS(BU29)+ABS(BL29)	=ABS(BV29)+ABS(BM29)
=ABS(BT30)+ABS(BK30)	=ABS(BU30)+ABS(BL30)	=ABS(BV30)+ABS(BM30)
=ABS(BT31)+ABS(BK31)	=ABS(BU31)+ABS(BL31)	=ABS(BV31)+ABS(BM31)

Vita

Derrick Lynn Baird was born in Detroit, Michigan the 11th day of July in 1973. He has lived in East Tennessee since 1973 and graduated from Campbell County Comprehensive High School in 1991. To obtain funds for college he enlisted in the Tennessee Army National Guard for a period of seven years.

Derrick received a B.S. in Mechanical Engineering in 1997 from the University of Tennessee. Currently he works as a Design Engineer for an Engineering Firm in Knoxville, TN.